Classification: PHYSICAL SCIENCES; Earth, Atmospheric, and Planetary Sciences

Title: Low gradient, single-threaded rivers prior to greening of the continents

Authors: Vamsi Ganti[a,b,1], Alexander C. Whittaker[c], Michael P. Lamb[d], and Woodward W. Fischer[d]

Author Affiliations:

[a]Department of Geography, University of California Santa Barbara, Santa Barbara, CA, USA 93106.

[b]Department of Earth Science, University of California Santa Barbara, Santa Barbara, CA, USA 93106.

[c]Department of Earth Science and Engineering, Imperial College London, London, UK SW7 2AZ.

[d]Division of Geological and Planetary Sciences, California Institute of Technology, Pasadena, CA, USA 91125.

[1]**Corresponding author**: Vamsi Ganti, 4810 Ellison Hall, University of California Santa Barbara, Santa Barbara, CA USA 93106; vganti@ucsb.edu; phone: +1 805-893-5991

Keywords: pre-vegetation alluvium; cross-stratification; Neoproterozoic Era

Abstract

The Silurian-age rise of land plants is hypothesized to have caused a global revolution in the mechanics of rivers. In the absence of vegetation-controlled bank stabilization effects, pre-Silurian rivers are thought to be characterized by shallow, multi-threaded flows, and steep river gradients. This hypothesis, however, is at odds with the pancontinental scale of early Neoproterozoic river systems that would have necessitated extraordinarily high mountains if such river gradients were commonplace at continental scale, which is inconsistent with constraints on lithospheric thickness. To reconcile these observations, we generated new estimates of paleogradients and morphologies of pre-Silurian rivers using a well-developed quantitative framework based on the formation of river bars and dunes. We combined data from previous work with original field measurements of the scale, texture and structure of fluvial deposits in Proterozoic-age Torridonian Group, Scotland—a type-example of pancontinental, pre-vegetation fluvial systems. Results showed that these rivers were low sloping (gradients 10^{-5} to 10^{-4}), relatively deep (4–15 m), and had morphology similar to modern, lowland rivers. Our results provide mechanistic evidence for the abundance of low gradient, single-threaded rivers in the Proterozoic eon, at a time well prior to the evolution and radiation of land plants—despite the absence of muddy and vegetated floodplains. Single-threaded rivers with stable floodplains appear to have been a persistent feature of our planet despite singular changes in its terrestrial biota.

Significance Statement

The origin of low-gradient meandering rivers—the primary conduits of water, carbon and nutrients in present-day terrestrial landscapes—is considered coeval with Silurian-age plant evolution. It was hypothesized that pre-Silurian rivers lacked bank strength and were dominantly steep and braided, implying vastly different transport capacities of water and sediment. This idea, however, is inconsistent with the super-continental-scale drainage of Neoproterozoic rivers, which requires unrealistically high mountains to achieve the necessary river gradients. Using geologic observations and quantitative paleohydraulic analyses, we show that pre-Silurian rivers were low-gradient, deep, and single-threaded—similar to modern meandering rivers. Results demonstrate uniformity of fluvial morphology despite a global revolution in Earth's terrestrial biota, with ramifications for the topographic signature of life on Earth and other planets.

\body

Photosynthesis has profoundly influenced the processes and environments at or near the Earth's surface, including the Great Oxygenation Event (1); it is also responsible for fundamental changes in the transport of sediment from the continents and its accumulation in basins. The colonization of terrestrial landscapes by land plants since *ca*. 450 Ma (2, 3) left its mark in the composition of deposits, with the pre-Silurian fluvial strata showing a distinctive lack of alluvial mudstones—a feature common in younger fluvial deposits (4). Land plants are also thought to have irreversibly changed the planform morphology of large rivers from a 'sheet-braided' style to the more commonly observed sinuous, meandering mode (5–7). Pre-Silurian rivers are hypothesized to be characterized by relatively steep, shallow, unconfined flows with multiple channel threads and unstable banks (5–9). For example, existing estimates of Proterozoic fluvial gradients span 4×10^{-3} to 4×10^{-2} (*SI Appendix*), which are two-to-three orders-of-magnitude steeper than modern continental-scale lowland rivers. These estimates are consistent with present-day observations, in which braided rivers are steeper than meandering rivers of the same water discharge (10), but raise an apparent paradox about the geodynamics of the Proterozoic Earth. Some Neoproterozoic rivers were pancontinental in size; provenance analyses indicate that major early Neoproterozoic rivers draining the Grenville orogen on the supercontinent Rodinia were >3000 km long (11). To achieve the estimated river gradients, continents would require >12 km relief—elevations significantly larger than any modern or previously recognized ancient orogens. This would have necessitated extraordinarily thick continental lithosphere, and is inconsistent with evidence that Neoproterozoic lithospheric thickness was likely similar to modern values (12).

These observations reveal a discordance between the inferred surficial environments in a pre-vegetation world and the geodynamical state of the Proterozoic Earth. Assemblages of tabular and laterally continuous sandstones in pre-Silurian fluvial deposits have been used to support the 'sheet-braided' hypothesis (5, 13–15), in addition to experiments that required vegetation-induced bank strength to elicit meandering (16, 17), and an increase in point-bar deposits associated with meandering since Silurian time (8). However, others have argued that some pre-Silurian rivers were deep (18–20) based on channel-body dimensions similar to modern single-threaded unvegetated rivers (21, 22), raising the possibility that they also could have had low gradients. Moreover, the existence of sinuous, meandering channels in desert landscapes (21–23), extraterrestrial deposits (like those seen on Mars)(24), and experiments with muddy cohesive banks (25), implies that single-threaded rivers can exist devoid of vegetation. Despite the ongoing debate as to how land plants changed the planform morphology of rivers (26–29), little work has focused on quantitative reconstructions of pre-Silurian river gradients. Thus, the apparent paradox between putative steep pre-Silurian river gradients and the scale of ancient orogens has yet to be reconciled. In addition, by quantifying river gradients it becomes possible to compare pre-Silurian river geometries to a mechanistic theory for the onset of river braiding (30). This further provides an assessment of river planform morphology independent of the typical approach using the deposit architecture of ancient rocks that has produced differing interpretations (e.g., 26, 27). Ultimately, quantitative reconstructions of pre-Silurian river morphology are needed to understand the routing and storage of water, sediment, carbon and nutrients—processes that maintain a habitable planet—on the early Earth and on extraterrestrial environments devoid of land plants.

Here, we generated new estimates of the paleogradients and morphologies of pre-Silurian rivers based on a suite of quantitative, paleohydraulic relations enabled by recent advances in the understanding of processes that form river bars and dunes. This approach differs considerably from that used by previous workers who estimated steep gradients based on empirical scaling relationships of present-day rivers with the *a priori* assumption that pre-Silurian rivers were bedload-dominated systems that lacked cohesive bank strength (*SI Appendix*). That logic presumes the validity of the sheet-braided hypothesis, rather than providing a test of it. By contrast, our calculations were based on original field measurements of bar and dune deposits in the Torridonian Group, Scotland—a type-example of pre-vegetation fluvial system—and compilation of data from other pre-Silurian fluvial deposits worldwide. Contrary to the sheet-braided hypothesis, results provide evidence for the abundance of low-gradient, single-threaded rivers prior to greening of the continents.

Deposits of a Pancontinental, Pre-vegetation Fluvial System: The Torridonian Sandstone

We studied the well-documented, classic fluvial sandstones in northwest Scotland known as the Torridonian Group (Fig. 1). These sedimentary rocks comprise an exceptionally and almost complete Middle to Upper Proterozoic succession of clastic, fluvial deposits, largely unmetamorphosed and undeformed, which rests unconformably on both Archean to Lower Proterozoic gneissic basement and tilted Mesoproterozoic strata of the Stoer Group (31) (Fig. 1).

The > 6 km thick sedimentary succession is dominated by the ubiquity of tabular- and trough-cross bedded sandstones in its upper to middle parts. Geochronological studies have constrained the onset of Torridonian sedimentation to early Neoproterozoic time (*SI Appendix*). We focused our analyses on two dominant formations within the group, the Applecross Formation (*ca*. 3 km thick) and the conformably overlying Aultbea Formation (> 2 km thick)(31) (Fig. 1). Following previous work within the Applecross Formation (32), we adopted two sampling intervals to provide a relative stratigraphic framework. These two sub-units, defined by their stratigraphic height above the underlying Lewisian Gneiss, are the 'Lower Applecross' (LAF) (~500 to 1000 m) and 'Upper Applecross' (UAF) (~2000 to 3000 m) (Fig. 1). This sampling strategy provides information averaged over similar stratigraphic thicknesses.

In alluvial rivers, the interactions between bed topography, sediment transport and fluid flow result in the formation of dynamic repeating topographic features such as ripples, dunes and bars—all called bedforms. The migration of bedforms results in the development of cross-stratification in the sedimentary record (33–35), which are primary indicators of paleoflow and sediment transport conditions. In the field, we measured 1724 individual cross-set thicknesses across 226 individual sets, median grain-size (D_{50}), and paleocurrent vectors at > 150 individual sets across 51 localities, evenly distributed among our stratigraphic sampling intervals (Figs. 1, 2, *SI Appendix*, Figs. S1-S3; Table S1). The results demonstrated a monotonic increase in set thicknesses over time, with $d_m = 0.21 \pm 0.14$ m (mean $\pm 1\sigma$), 0.56 ± 0.31 m, and 0.66 ± 0.35 m for LAF, UAF, and Aultbea Formation, respectively (Figs. 2G, *SI Appendix*, Fig. S4). The increase in d_m was concomitant with a decrease in D_{50} (Fig. 2H); D_{50} is 2.25 ± 0.75 mm (mean $\pm 1\sigma$) (particle sizes of very coarse sand to granules), 1.5 ± 0.12 mm (very coarse sand), and 0.7 ± 0.5 mm (medium to coarse sand) for LAF, UAF, and Aultbea Formation, respectively.

Paleocurrent vector data confirmed a dominant east-southeast paleoflow direction (31, 32), with no trend across stratigraphic intervals (Fig. 1C).

Morphological Reconstruction of Pre-vegetation Rivers

In agreement with prior studies of the Torridonian Group (31, 32), we interpreted the observed cross-stratification as fluvial dune deposits, which is supported by observations of steep cross-bed dip angles (*SI Appendix*, Fig. S5), typical of modern dune lee-face angles (36), and presence of larger, rare barform deposits that represent higher-order fluvial hierarchical elements (*SI Appendix*, Figs. S6, S7). Numerical and experimental studies revealed that a strong relationship exists, given by $h_d = (2.9 \pm 0.7)d_m$, between d_m and mean bedform heights (h_d); this is well-constrained across a wide range of aggradation and migration rates of subcritically-climbing bedforms (33–35). Thus, our observed increase in d_m reflects an increase in formative dune heights (*Materials and Methods and SI Appendix*; Figs. S8, S9). The dune heights scale with the boundary layer thickness, which is approximated by the flow depth (H) in open-channel flows (36). An extensive field and experimental data compilation constrained the h_d-H scaling relation, given by $H = 6.7h_d$, with the first and third quartiles of H given by $4.4h_d$ to $10.1h_d$, respectively (36). Using this empirical observation, the estimated median values of H for LAF, UAF, and Aultbea rivers were 4.1 ± 1 m ([2.7,6.2] m, 1st and 3rd quartiles of H), 11 ± 2.7 m ([7.2,16.5] m), and 12.8 ± 3.1 m ([8.4,19.4] m), respectively (Fig. 3A, *Materials and Methods*). These data are inconsistent with the sheet-braided hypothesis that predicts shallow flows in Neoproterozoic rivers (5, 6), but instead show that deep flows characterized well-known Proterozoic rivers (18–20).

The ubiquity of cross-bedded sandstones indicates that fluvial dunes were stable and pervasive during Torridonian sedimentation. Several studies have formulated a graphical framework that establishes the hydraulic and sediment transport conditions for the stable existence of fluvial dunes (e.g., 37), parameterized by the Froude number, particle Reynolds number, and Shields stress ($\tau^* = \tau_b/\rho R g D_{50}$, where ρ is the density of water, g is gravitational acceleration, τ_b is bed shear stress, and R = 1.65 for quartz). We used a bedform stability diagram (38) to place bounds on the range of τ^* (*SI Appendix*; Fig. S10), and approximated τ_b assuming steady, uniform flow ($\tau_b = \rho g H S$) to estimate a distribution of paleoslope (S) values using Monte Carlo sampling (*Materials and Methods*). These results show that the Torridonian Group was deposited by gently sloping rivers, and S decreased from the older to the younger stratigraphic units. The estimated median value (and 1st and 3rd quartiles) of S for LAF, UAF, and Aultbea rivers were $3.9\text{x}10^{-4}$ ([$2.0\text{x}10^{-4}$, $7.1\text{x}10^{-4}$]), $9.7\text{x}10^{-5}$ ([$4.4\text{x}10^{-5}$, $1.9\text{x}10^{-4}$]), and $4.5\text{x}10^{-5}$ ([$2.0\text{x}10^{-5}$, $9.2\text{x}10^{-5}$]), respectively (Fig. 3B). The estimated S values for the Torridonian Group are similar to modern continental, lowland and foreland-basin rivers. To confirm this result we constrained S independently, using an empirical relationship based on the bankfull Shields stress criteria observed in modern alluvial rivers (39). This approach yielded similar values for paleoslope, supporting the estimates derived from bedform stability diagram, and implying that Proterozoic rivers had gradients similar to modern rivers (Fig. 3B).

Modern low-gradient, continental rivers are bounded by floodplains, in contrast to the sheet-braided hypothesis where floodplains would be absent. Quantifying floodplain facies in pre-vegetation alluvium is challenging, considering the lack of bioturbation and fossils, absence of mudstones, and limited outcrop extent (40). However, recent work has documented mature floodplain systems with bedsets > 10 m in thickness throughout the Proterozoic eon (40). In the Applecross Formation, floodplain facies composed of ripple-laminated heterolithic beds, sets that thin away from the channel bank, and rare preserved channel levees have been documented (20, 40). Thus, like modern continental rivers, pre-Silurian rivers did have floodplains, but they were coarser-grained than their modern counterparts possibly due to vegetation's role in baffling overbank flows and binding mud deposits (4, 40).

Were Pre-vegetation Rivers Single-threaded or Braided?

Sheet-braided hypothesis requires large channel width-depth ratios to trigger the onset of braiding (30). We constrained the aspect ratio of Torridonian rivers by examining the water balance at both the channel and catchment scales (*Materials and Methods and SI Appendix*, Fig. S11). Water discharge was equated to the product of flow width (W), depth (H), and velocity (U) at a given a location; it is also related to the average precipitation rate (P) and the area over which this rainfall accumulates to contribute to the streamflow (A) (*Materials and Methods*). Using these mass balance constraints, previous estimates of A (32, 41), and our reconstructions of H and S (Figs. 3A,B), we found that $W/H \in [10, 100]$ for $10^4 \leq A \leq 10^6$ km^2 (Fig. 3C), and the data reside in the stability field for single-threaded, rather than braided, rivers (Fig. 3D). UAF and Aultbea rivers could only have exceeded the threshold of 10 braided threads, as implied by the sheet-braided hypothesis, for unrealistic values of A >10^8 km^2 (i.e., river lengths > Earth's circumference) or P >10 m/yr that would be tenfold the precipitation in the modern Inter-Tropical Convergence Zone (*Materials and Methods*). The predominance of >100 m lateral continuity of Applecross sandbodies (32) was previously used to support the sheet-braided hypothesis, but these dimensions are consistent with channel belts from single-threaded rivers given our estimates of channel depths and width-depth ratios.

Did low-gradient, deep rivers persist throughout the Proterozoic eon? We compiled reported cross-set thickness for 10 fluvial formations throughout the Proterozoic eon (*SI Appendix*), and estimated H and S in a similar way as the Torridonian Group (Figs. 3A,B). For the global compilation, H ranged from 4 to 15 m and S was on the order of 10^{-4} (Fig. 4), indicating that low-sloping, deep rivers persisted throughout Proterozoic time.

While vegetation is hypothesized to be the primary control on bank strength that allows small width-depth ratios for post-Silurian single-threaded rivers (5, 6), other mechanisms for bank strength are needed to explain single-threaded pre-Silurian rivers. Mud and fine-grained sediments can, in principle, provide the required cohesive bank strength (23, 25); however, the mineralogy of Applecross sandstones indicates that mud was rare (31). Microbial mats and biofilms can also provide cohesion to unconsolidated sand, and microbial sedimentary structures are prevalent in the Torridonian Supergroup (42). Experimental studies demonstrated that microbially-bound medium-to-coarse sand can withstand a shear stress between 0.3 to 4 Pa without significant grain movement (43). The estimated range of τ_b for the Torridonian rivers was 0.2 to 10 Pa (Figs. 3A,B), suggesting that microbial stabilization of bank sediment could have sustained deep flows with relatively high τ_b during the Proterozoic eon. Regardless of the bank stabilization mechanism, our results point to the abundance of low-gradient, deep, single-threaded rivers, and imply a typical degree of relief for pancontinental river systems prior to the evolution of plants.

Materials and Methods

Stratigraphic correlation and sedimentological context. Our fieldwork focused on the Applecross and Aultbea Formations of the Torridonian Group (Fig. 1; *SI Appendix*). The basal Diabeg Formation of the group was not sampled, but its distinctive stratigraphic position, lying within incised paleo-valleys in the Lewisian Gneiss, was used as a marker to evaluate the stratigraphic position of key localities within the Applecross Formation, below. Our interpretations necessarily rest on collection of sedimentological data from appropriatelyidentified stratigraphic intervals within the Torridonian Group. All sampling localities, including the type sections, were located carefully in the field with reference to 1) the British Geological Survey (Scotland) maps at 1:50000 and 1:63360 scale; 2) the Geological Society of London memoir of Stewart (31), which provides an in-depth "directory" of key localities; 3) field sites described in Table 1 of Nicholson (32); 4) and from previous field campaigns in northwest Scotland by ACW. Sites were visited over two field seasons in September 2016 and 2017. The Applecross Formation makes up the majority of the Torridonian Group and consists of >3 km of coarse red sandstones, pebbly in sections particularly toward the base, which are ubiquitously planar and trough cross-bedded. We adopted the informal sub-division of Nicholson (32) and Stewart (31), and collected data from the formation in two groupings, one towards the base and one towards the top of the formation respectively, referred to as the 'Lower Applecross' (LAF) and 'Upper Applecross' (UAF). The LAF is easily recognized where it overlies the distinctive Diabeg Formation; we use an interval of approximately 500–1000 m above the lower basal unconformity of the Lewisian to constrain this unit. The UAF refers to sediments in the Applecross Formation underlying the Aultbea Formation and located approximately 2000–3000 m above the base of the Torridonian Group.

At the majority of field localities, planar to trough cross bedded sandstones, typically in coarse to very coarse sand (sometimes at granule grade in the LAF), comprise the dominant facies association, and represent the migration of fluvial dunes, worked by sustained subcritical flows within active channels (*SI Appendix*, Figs. S1-S3). Many of these cross-bedded horizons can be traced for over tens of meters, giving the Torridonian Sandstone its distinctive character. Mud-size sediment is generally absent. In the Aultbea Formation a further facies association consists of medium sandstones with marked soft sediment deformation, which overprints recognizable trough cross-bedding to a lesser or greater degree, and is interpreted to represent sediment liquefaction and/or water escape (*SI Appendix*, Fig. S3). Other elements of facies architecture include occasional bar forms (*SI Appendix*, Figs. S6, S7) and rare channel bodies (20). Interpreted bar forms in the Torridonian Group have a planar to mildly-erosive base and fine upwards over length scales of several meters. They show changes in sedimentary structures from thicker, tabular or trough cross-bedding near the base, representing dunes to smaller ripple cross-beds at the bar top, where preserved. Evidence of lateral accretion consists of smaller cross-sets climbing on the bar flanks. Lateral accretion surfaces themselves dip at angles of <10 degrees when corrected for depositional dip, markedly shallower than the trough cross bedding (*SI Appendix,* Fig. S5). Cross-set thicknesses were measured at regular intervals within each set with a tape or rule from the asymptotic lower bounding surface to the erosional bounding surface at the top of the set, with a precision of ± 5 mm. This method required careful delineation of the cross-set boundaries, which we agreed in the field before measurement. A distribution of cross-set thicknesses was obtained for each cross set; at most localities multiple sets were measured (*SI* Appendix, Table S1). In total, 553, 602 and 569 thickness measurements were made for the LAF, UAF and Aultbea Formation, respectively. Grain size for the cross sets was constrained from the analysis of scaled field photographs (*SI Appendix*; Figs. S1-S3; Table S1). The dip and dip direction of planar cross bedding (or the trend and plunge of the center of trough cross beds, where necessary) was used to estimate paleo-flow direction. These measurements were corrected by the dip and dip direction of the depositional bedding at each locality using *Stereonet9*; the failure to correct for bedding can lead to spurious results, particularly where the dip angle of the cross-beds is less than that of the bedding.

Scaling bedform heights from cross-set thickness. Previous experimental (33, 44, 45) and numerical (34) work demonstrated that the ratio of the formative dune height to the mean set thickness is 2.9±0.7 for a range of aggradation and migration rates of subcritically-climbing bedforms. We used this scaling relationship to estimate the formative bedform heights (*SI Appendix*). We used the global mean of measured set thickness within each stratigraphic interval for this estimation (Fig. 2).

Scaling formative flow depths from estimated bedform heights. Empirical scaling relationships of bedform height (h_d) and flow depth (H) are based on linking dune dimensions to the boundary layer thickness, which is often assumed to be the flow depth in open channel flows. Based on >380 field observations of h_d and H, Bradley and Venditti (36) provided a scaling relation given by:

$$H = 6.7h_d \qquad (1)$$

It was also shown that 1st and 3rd quartiles of H were bound by $4.4h_d$ and $10.1h_d$. We used these estimates for constraining H (Fig. 3A). Comparison of these estimates with other methods outlined in literature showed good agreement (*SI Appendix*, Fig. S12).

Bedform stability and estimation of paleoslope. Previous work indicated that at least three dimensionless numbers are needed to describe the stability of fluvial bedforms (37). River dunes exist only in subcritical flow conditions (*SI Appendix*), i.e., Froude number (Fr) < 1, and bedform stability is independent of Fr for subcritical flows (*SI Appendix*). We used the bedform stability diagram proposed by Lamb et al. (38), which parameterized flow and sediment transport conditions using Shields stress and the particle Reynolds number, Re_p (*SI Appendix*, Fig. S10), to bound the formative Shields stress of Torridonian rivers. We estimated Re_p for each stratigraphic interval using our measurements of D_{50} (Fig. 2), and assumed the kinematic viscosity of water of $\nu = 10^{-6}$ m^2/s, which corresponds to a temperature of 20 °C. The estimated τ^* bounds are insensitive to ν over a range of 10 to 30 °C —a temperature range consistent with the inferred subtropical, semi-arid climate during Torridonian sedimentation (31).

We included the range of Shields stresses that correspond to the existence of dunes and also the transitional zone between dunes and upper plane beds (*SI Appendix*, Fig. S10). This is a conservative approach in that it represents the maximum possible range of τ^* for stable existence of river dunes. Once τ^* was bound for each stratigraphic sampling interval, we approximated τ_b as the depth-slope product, and the paleoslope, *S*, is given by

$$S = \frac{RD_{50}\tau^*}{H} \qquad (2)$$

in which $R = 1.65$ is the submerged specific density of sediment for quartz. We then estimated *S* using Monte Carlo simulations. We generated 10^7 random samples of τ^* (uniformly distributed within the bounds provided by the bedform stability diagram), and 10^7 normally distributed random samples of D_{50} given the mean and standard deviation of D_{50} across multiple localities within each stratigraphic sampling interval. Finally, we generated 10^7 random samples of *H* given the uncertainty in formative flow depths (36). This procedure yielded 10^7 random samples of *S* using equation (2), and we reported the median, 1st and 3rd quartiles, and the 9th and 91st percentiles in Figure 3B.

Finally, we validated the bedform stability diagram using a recent compilation of experimental and field data that documented different bedform states over a wide range of sediment transport and flow conditions (46). We reduced this compilation to the range of Re_p that span observations in the Torridonian Group, which resulted in 998 individual experimental data points and 47 field data points. This comparison indicates that the bedform stability diagram predicts the range of formative Shields stress reasonably well (*SI Appendix*, Fig. S10).

Estimation of paleoslope from modern scaling arguments based on bankfull Shields stress. Models for paleoslope estimation from stratigraphic observations of fluvial strata are based on the empirical observation that rivers organize their bankfull shear stress around a geomorphic threshold driven by the dominant transport mode of bed sediment. For example, at bankfull conditions in alluvial rivers, sand is barely suspended, while gravel is transported very near the threshold of motion (39). Based on a compilation of 541 bankfull measurements of alluvial rivers and Bayesian regression analysis, the following equation was proposed for estimating paleoslope of alluvial rivers (39):

$$\log S = \alpha_0 + \alpha_1 \log D_{50} + \alpha_2 \log H \quad (3)$$

where α_0 = -2.08±0.036 (mean ± 1σ), α_1 = 0.254±0.016, and α_3 = -1.09±0.044 are empirical constants, and H and D_{50} are measured in m. We used Monte Carlo simulations to constrain S using this independent method (Fig. 3B).

Constraining the aspect ratio of channels. We estimated the aspect ratio of the Torridonian rivers by performing water balance at reach- and catchment-scale (47), and using constraints on precipitation rate, P, drainage area, A, and depth-averaged flow velocity, U. Mass balance dictates that the water discharge, Q, satisfies the following relation:

$$Q = UWH \quad (4)$$

in which W is the width of the channel. Under the assumption of normal flow conditions:

$$U = \sqrt{\frac{gHS}{C_f}} \qquad (5)$$

where C_f is a dimensionless friction coefficient that is a function of the ratio of D_{50} and H. Following previous work (48), we assumed $C_f \approx 0.01$; however, using a more elaborate friction law (49) results in C_f values that range between 10^{-3} and 10^{-2}. Since U is inversely proportional to the square-root of C_f (equation 5), we used the simplest formulation of a constant C_f because the variability in our data supersedes these differences. The estimated U using $C_f \approx 0.01$ is consistent with the bedform stability diagram expressed in terms of U and D_{50} (*SI Appendix*, Fig. S10C) (50). We estimated *Fr*, which is required for assessment of the planform stability of rivers (Fig. 3D)(30), using $C_f \approx 0.01$ and through Monte Carlo sampling where 10^7 random samples of H and S were generated as described previously (*SI Appendix*).

Water discharge can also be related to the precipitation rate and drainage area through the following relation:

$$Q = cPA \qquad (6)$$

where $c \in [0,1]$ and accounts for infiltration, evaporation, and attenuation of the rainfall pulse within a drainage basin. Combining equations (4-6) and rearranging results in an expression for the channel width, W, given by:

$$W = cPA\sqrt{\frac{C_f}{gSH^3}} \qquad (7)$$

In equation (7), sedimentological data and paleohydraulic analyses provide constraints on S, H, and C_f. Thus, the aspect ratio of the channels can be constrained if we can bound the values of c, P, and A, which we discuss individually next.

Constraints on precipitation rates. Data from paleomagnetism studies suggest that the Applecross and Aultbea Formations were deposited in subtropical to temperate regions with paleolatitude estimates ranging from 30° to 50° S, consistent with the inferred paleoclimate from the modal feldspar and quartz content of the Applecross sandstones (31). The modern precipitation rates are greatest within 15° of the equator and the subtropical and temperate regions receive approximately five times less rainfall than the tropical regions, on average (51). The precipitation maximum within the tropics is associated with the ascending branch of the Hadley circulation (52) and the drier climates in the subtropics and temperate regions are associated with the drier descending air of the same Hadley circulation. Geologic and paleomagnetic data spanning the last 2 billion years indicate that this descending circulation is a persistent feature of the Earth's climate (53), indicating that modern precipitation data may provide a reasonable first-order proxy for P in equation (7). We constrained P using a recent data compilation that demonstrated that P is symmetric around the Earth's equator, and the subtropical and temperate regions receive rainfall between 0.5 to 1 m/yr (51).

To test the veracity of equation (6) and constrain c, we compiled data of monthly water discharge data, Q, and drainage area, A, for modern continental-scale rivers that reside in the subtropical and temperate regions (54). Our compilation includes data from 29 rivers such as the MacKenzie, Nelson, Yukon, Mississippi, Missouri, Parana, Danube, Lena, Murray, and Indus. We then assumed $P \in [0.5,1]$ m/yr, which represents the full range of observed average precipitation rates in the subtropical and temperate regions (51). Our data compilation validated equation (6) and constrained the value of c between 0.1 and 1 (*SI* Appendix, Fig. S11). Only one data point in our compilation does not lie within these bounds, which corresponds to the Murray River, Australia, where evapotranspiration and infiltration rate is greater than the precipitation rate. Thus, equation (6) with $c \in [0.1, 1]$ provides an estimate of the maximum possible water discharge. This framework is valid for fluvial systems that experience either flashy or more uniform hydrographs.

Constraints on drainage area. The age distributions of detrital zircons from the Applecross and Aultbea Formations were documented to be similar, suggesting that they were part of the same depositional system (55). Moreover, the conformable nature and the overall upward fining sequence of Applecross and Aultbea Formations (Fig. 2H) suggest that the UAF and Aultbea Formation were more distal parts of the same sediment routing system, compared to the LAF (31, 32). Previous workers argued that the Torridonian Group was deposited by a late- to post-Grenvillian foreland trunk river system, near the middle of supercontinent Rodinia (31, 55). Thus, the drainage area likely increased monotonically from LAF to the Aultbea Formation. Previous workers (32, 41) have inferred a drainage area of $1 - 2 \times 10^4$ km^2 for the LAF rivers, and Nicholson (32) estimated a drainage area of $>10^5$ km^2 for the UAF rivers. We interrogated the aspect ratio of the Torridonian rivers for A of 10^4 to 10^7 km^2 (Fig. 3C). The lower bound on A is consistent with previous estimates for LAF (32, 41), and the upper bound on A is twice the drainage area of the Amazon, the largest drainage area of present-day rivers.

Estimation of aspect ratio of flows. We used equation (7) to estimate W, and the aspect ratio of the Torridonian rivers. Similar to paleoslope estimation, we generated 10^7 random samples of S for LAF, UAF, and Aultbea Formation using equation (2) and H using methods described earlier. We assumed $C_f = 0.01$, and generated 10^7 random samples of P, uniformly distributed and bound by 0.5 and 1 m/yr. We also generated 10^7 random samples of *c*, uniformly distributed and bound by 0.1 and 1 (*SI* Appendix, Fig. S11). We then evaluated *W* for four values of *A*: 10^4, 10^5, 10^6 and 10^7 km^2, for each stratigraphic sampling interval (Fig. 3C). Consistent with previous studies (32, 41), our independent analyses suggests that $W > H$ for drainage areas in excess of 10^4 km^2 and 10^5 km^2 for LAF and UAF, respectively. Finally, we used the same Monte Carlo sampling approach to estimate *S/Fr* and *H/W* for the assessment of the planform stability of Torridonian rivers for different values of *A* (Fig. 3D). We did not estimate *W* for $A > 10^7$ km^2. River length (*L*) and *A* in present-day rivers are related through the following relation: $L = 1.4A^{0.6}$ (56), where *L* and *A* are in miles and square miles, respectively. Using this scaling argument, $A = 10^8$ km^2 corresponds to $L \approx 80{,}000$ km, which is twice the Earth's equatorial circumference. Drainage areas of 10^4, 10^5, 10^6 and 10^7 km^2 correspond to river lengths of approximately 300 km, 1200 km, 5000 km, and 20,000 km, respectively.

Acknowledgments: We thank F. Macdonald, W. McMahon, and S. Gupta for fruitful discussions. V. G. acknowledges funding from the Imperial College London Junior Research Fellowship.

References

1. Fischer WW, Hemp J, Johnson JE (2016) Evolution of Oxygenic Photosynthesis. *Annu Rev Earth Planet Sci* 44(1):647–683.

2. Kenrick PR, Crane PR (1997) The origin and early evolution of plants on land. *Nature* 389:33–39.

3. Morris JL, et al. (2018) The timescale of early land plant evolution. *Proc Natl Acad Sci* 115(10):201719588.

4. McMahon WJ, Davies NS (2018) Evolution of alluvial mudrock forced by early land plants. *Science (80-)* 359(6379):1022–1024.

5. Gibling MR, Davies NS (2012) Palaeozoic landscapes shaped by plant evolution. *Nat Geosci* 5(2):99.

6. Davies NS, Gibling MR (2011) Evolution of fixed-channel alluvial plains in response to Carboniferous vegetation. *Nat Geosci* 4:629.

7. Gibling MR, et al. (2014) Palaeozoic co-evolution of rivers and vegetation: A synthesis of current knowledge. *Proc Geol Assoc* 125(5–6):524–533.

8. Davies NS, Gibling MR (2010) Paleozoic vegetation and the Siluro-Devonian rise of fluvial lateral accretion sets. *Geology* 38(1):51–54.

9. Schumm SA (1968) Speculations Concerning Paleohydrologic Controls of Terrestrial Sedimentation. *GSA Bull* 79(11):1573–1588.

10. Leopold LB, Wolman MG (1957) *River Channel Patterns: Braided, Meanding, and Straight* (US Government Printing Office).

11. Rainbird RH, et al. (1997) Pan-Continental River System Draining Grenville Orogen Recorded by U-Pb and Sm-Nd Geochronology of Neoproterozoic Quartzarenites and Mudrocks, Northwestern Canada. *J Geol* 105(1):1–17.

12. Artemieva IM, Mooney WD (2001) Thermal thickness and evolution of Precambrian lithosphere: A global study. *J Geophys Res Solid Earth* 106(B8):16387–16414.

13. Cotter E (1977) The evolution of fluvial style, with special reference to the central Appalachian Paleozoic.

14. Long DGF (1978) Proterozoic stream deposits: some problems of recognition and interpretation of ancient sandy fluvial systems. *Fluv Sedimentol* 5:313–341.

15. Davies N, Gibling M, Rygel M (2011) Alluvial facies evolution during the Palaeozoic greening of the continents: Case studies, conceptual models and modern analogues. *Sedimentology* 58(1):220–258.

16. Tal M, Paola C (2007) Dynamic single-thread channels maintained by the interaction of flow and vegetation. *Geology* 35(4):347–350.

17. Braudrick CA, Dietrich WE, Leverich GT, Sklar LS (2009) Experimental evidence for the conditions necessary to sustain meandering in coarse-bedded rivers. *Proc Natl Acad Sci* 106(40):16936–16941.

18. Ielpi A, Rainbird RH (2016) Reappraisal of precambrian sheet-braided rivers: Evidence for 1·9 Ga deep-channelled drainage. *Sedimentology* 63(6):1550–1581.

19. Ielpi A, Rainbird RH, Ventra D, Ghinassi M (2017) Morphometric convergence between Proterozoic and post-vegetation rivers. *Nat Commun* 8:15250.

20. Ielpi A, Ghinassi M (2015) Planview style and palaeodrainage of Torridonian channel belts: Applecross Formation, Stoer Peninsula, Scotland. *Sediment Geol* 325:1–16.

21. Ielpi A (2017) Lateral accretion of modern unvegetated rivers: Remotely sensed fluvial-aeolian morphodynamics and perspectives on the Precambrian rock record. *Geol Mag* 154(3):609–624.

22. Ielpi A (2018) Morphodynamics of meandering streams devoid of plant life: Amargosa River, Death Valley, California. *GSA Bull*. doi:https://doi.org/10.1130/B31960.1.

23. Ielpi A, Lapôtre MGA (2018) Biotic forcing militates against river meandering in the

modern Bonneville Basin of Utah. *Sedimentology* 0(ja). doi:10.1111/sed.12562.

24. Burr DM, et al. (2009) Pervasive aqueous paleoflow features in the Aeolis/Zephyria Plana region, Mars. *Icarus* 200(1):52–76.

25. Peakall J, Ashworth PJ, Best JL (2007) Meander-Bend Evolution, Alluvial Architecture, and the Role of Cohesion in Sinuous River Channels: A Flume Study. *J Sediment Res* 77(3):197–212.

26. Ielpi A, Ghinassi M, Rainbird RH, Ventra D (2018) Planform sinuosity of Proterozoic rivers: A craton to channel-reach perspective. *Fluv Meand their Sediment Prod rock Rec (IAS SP 48)* 48:81–118.

27. McMahon WJ, Davies NS (2018) The shortage of geological evidence for pre-vegetation meandering rivers. *Fluv Meand Their Sediment Prod Rock Rec*:119–148.

28. Davies NS, et al. (2017) Discussion on 'Tectonic and environmental controls on Palaeozoic fluvial environments: reassessing the impacts of early land plants on sedimentation' Journal of the GeologicalSociety, London, https://doi.org/10.1144/jgs2016-063. *J Geol Soc London* 174(5):947–950.

29. Santos MGM, Mountney NP, Peakall J (2016) Tectonic and environmental controls on Palaeozoic fluvial environments : reassessing the impacts of early land plants on sedimentation. *J Geol Soc London* 174:393–404.

30. Parker G (1976) On the cause and characteristic scales of meandering and braiding in rivers. *J Fluid Mech* 76(3):457–480.

31. Stewart AD (2002) The later Proterozoic Torridonian rocks of Scotland: their sedimentology, geochemistry and origin. *Geological Society, London* (Geological Society

of London), p 132.

32. Nicholson PG (1993) *A basin reappraisal of the Proterozoic Torridon Group, northwest Scotland* (International Association of Sedimentologists).

33. Leclair SF, Bridge JS (2001) Quantitative Interpretation of Sedimentary Structures Formed by River Dunes. *J Sediment Res* 71(5):713–716.

34. Jerolmack DJ, Mohrig D (2005) Frozen dynamics of migrating bedforms. *Geology* 33(1):57–60.

35. Paola C, Borgman L (1991) Reconstructing random topography from preserved stratification. *Sedimentology* 38(4):553–565.

36. Bradley RW, Venditti JG (2017) Reevaluating dune scaling relations. *Earth-Science Rev* 165:356–376.

37. Southard JB (1991) Experimental Determination of Bed-Form Stability. *Annu Rev Earth Planet Sci* 19(1):423–455.

38. Lamb MP, Grotzinger JP, Southard JB, Tosca NJ (2012) Were Aqueous Ripples on Mars Formed by Flowing Brines? *Sedimentary Geology of Mars*, eds Grotzinger JP, Milliken RE (SEPM Society for Sedimentary Geology). Available at: https://doi.org/10.2110/pec.12.102.0139.

39. Trampush SM, Huzurbazar S, McElroy B (2014) Empirical assessment of theory for bankfull characteristics of alluvial channels. *Water Resour Res* 50(12):9211–9220.

40. Ielpi A, et al. (2018) Fluvial floodplains prior to greening of the continents: Stratigraphic record, geodynamic setting, and modern analogues. *Sediment Geol* 372:140–172.

41. Williams GE, Foden J (2011) A unifying model for the Torridon Group (early Neoproterozoic), NW Scotland: Product of post-Grenvillian extensional collapse. *Earth-Science Rev* 108(1–2):34–49.

42. Prave AR (2002) Life on land in the Proterozoic: Evidence from the Torridonian rocks of northwest Scotland. *Geology* 30(9):811–814.

43. van de Lageweg WI, McLelland SJ, Parsons DR (2018) Quantifying biostabilisation effects of biofilm-secreted and extracted extracellular polymeric substances (EPSs) on sandy substrate. *Earth Surf Dynam* 6:203–215.

44. Ganti V, Paola C, Foufoula-Georgiou E, Foufoula-Georgiou E (2013) Kinematic controls on the geometry of the preserved cross sets. *J Geophys Res Earth Surf* 118(3):1296–1307.

45. Bridge JS (1997) Thickness of sets of cross strata and planar strata as a function of formative bed-wave geometry and migration, and aggradation rate. *Geology* 25(11):971–974.

46. Ohata K, Naruse H, Yokokawa M, Viparelli E (2017) New Bedform Phase Diagrams and Discriminant Functions for Formative Conditions of Bedforms in Open-Channel Flows. *J Geophys Res Earth Surf* 122(11):2139–2158.

47. Perron JT, et al. (2006) Valley formation and methane precipitation rates on Titan. *J Geophys Res E Planets* 111(11). doi:10.1029/2005JE002602.

48. Métivier F, Lajeunesse E, Devauchelle O (2017) Laboratory rivers: Lacey’s law, threshold theory, and channel stability. *Earth Surf Dyn* 5(1):187–198.

49. Parker G, Wilcock PR, Paola C, Dietrich WE, Pitlick J (2007) Physical basis for quasi-universal relations describing bankfull hydraulic geometry of single-thread gravel bed

rivers. *J Geophys Res Earth Surf* 112(4). doi:10.1029/2006JF000549.

50. Carling PA (1999) Subaqueous gravel dunes. *J Sediment Res* 69(3):534–545.

51. Macdonald FA, Swanson-Hysell NL, Park Y, Lisiecki L, Jagoutz O (2019) Arc-continent collisions in the tropics set Earth's climate state. *Science (80-)*.

52. Hadley G. (1735) Concerning the cause of the general trade-winds. Royal Soc. London Philos. Trans., 29:58–62. *Philos Trans* 39(437):58–62.

53. Evans DAD (2006) Proterozoic low orbital obliquity and axial-dipolar geomagnetic field from evaporite palaeolatitudes. *Nature* 444(7115):51–55.

54. Vorosmarty CJ, Fekete BM, Tucker BA (1998) Global River Discharge, 1807-1991, V[ersion]. 1.1 (RivDIS). doi:10.3334/ornldaac/199.

55. Rainbird RH, Hamilton MA, Young GM (2001) Detrital zircon geochronology and provenance of the Torridonian, NW Scotland. *J Geol Soc London* 158(1):15–27.

56. Hack JT (1957) *Studies of longitudinal stream profiles in Virginia and Maryland* doi:10.1016/j.ejpoleco.2003.07.001.

57. Blair TC, McPherson JG (1994) Alluvial fans and their natural distinction from rivers based on morphology, hydraulic processes, sedimentary processes, and facies assemblages. *J Sediment Res* 64(3a):450–489.

Figure Legends

Fig. 1. Location and stratigraphy of the Torridonian Group. A) Location of exposures of Torridonian Sandstone and a simplified stratigraphic section of the Torridonian Group. B) Detailed location of exposures of Applecross (pink) and Aultbea Formation (orange). The filled

markers (light orange – LAF, purple – UAF, and green – Aultbea Formation) indicate the field localities where set thickness and grain size data were measured. C) Rose diagram of the paleocurrent vectors for each stratigraphic sampling interval (*Materials and Methods*).

Fig. 2. Summary of field data collected for the Torridonian Group. A–C) Cross-stratification in the Lower Applecross, Upper Applecross, and the Aultbea Formation, respectively. The solid and dashed lines indicate cross-bedding and the interpreted erosional boundaries, respectively (*Materials and Methods and SI Appendix*, Figs. S1-S3). D–F) Macro photographs showing the reduction in grain size from the Lower Applecross to the Aultbea Formation (*SI Appendix*, Figs. S1-S3). Cumulative distribution function of the measured set thickness (G) and median grain-size (H) at individual outcrops within the stratigraphic sampling intervals.

Fig. 3. Paleohydraulic reconstruction for the Torridonian Group demonstrates that these ancient rivers were low-sloping and single-threaded. A) Estimated formative flow depth, H, for the Applecross and Aultbea Formations (*Materials and Methods and SI Appendix*). B) Estimated S from bedform stability diagrams (38) (filled boxplots) and modern scaling arguments (open boxplots) (39) (*Materials and Methods*). Gray shaded area denotes the natural depositional slope gap between alluvial fans and rivers (57). C) Estimated W/H of the Torridonian rivers as a function of A (*Materials and Methods and SI Appendix*, Fig. S11). D) Theoretical stability fields of fluvial planform morphology along with supporting data from modern fluvial environments (30). Reconstructed data of the Torridonian rivers for four decades of drainage area; colored markers and error bars indicate the median and the interquartile range, respectively (*Materials and Methods*). The solid, thick line indicates the theoretical prediction of the transition from single-threaded to braided planform morphology.

Fig. 4. Estimated flow depths and paleo-fluvial gradients for a global compilation of Proterozoic rivers. A) Formative flow depths for 10 fluvial formations throughout the Proterozoic eon (*Materials and Methods and SI Appendix*). B) Estimated fluvial gradients from bedform stability diagram (filled boxplots) and modern scaling arguments (open boxplots), similar to Figure 3B (*Materials and Methods*). The shaded gray area indicates the natural depositional slope gap between modern alluvial rivers and alluvial fans (57). The histogram shows a worldwide compilation of gradients for modern rivers and alluvial fans (*SI Appendix*).

This article contains **supporting online information**.

Author contributions: VG: conceptualization, fieldwork, paleohydraulic analyses, data interpretation and writing. ACW: conceptualization, fieldwork, data interpretation and writing. MPL: conceptualization, paleohydraulic analyses, data interpretation, and writing. WWF: conceptualization, data interpretation, and writing.

Code and Data availability: All data generated or analyzed during this study are included in Supplementary Online Material.

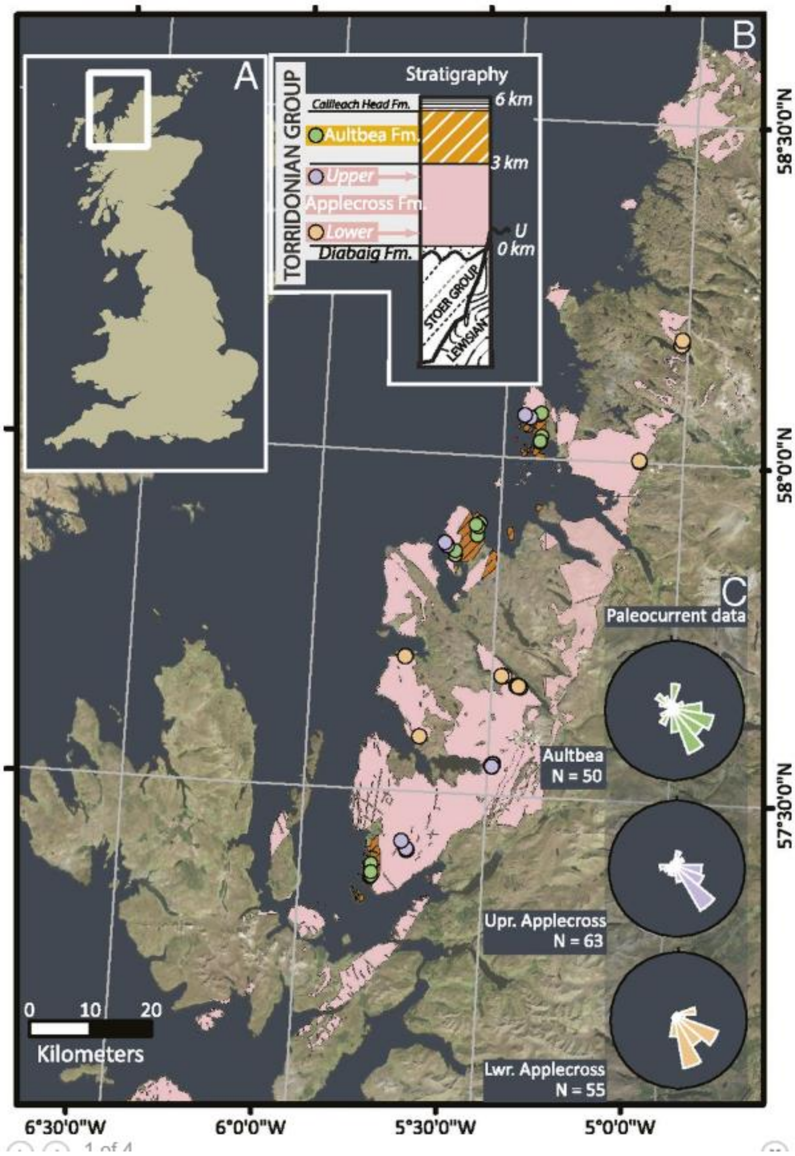

A
B
Stratigraphy
TORRIDONIAN GROUP
Calleach Head Fm.
Aultbea Fm.
Upper
Applecross Fm.
Lower
Diabaig Fm.
6 km
3 km
U
0 km
STOER GROUP
LEWISIAN
C
Paleocurrent data
Aultbea
N = 50
Upr. Applecross
N = 63
Lwr. Applecross
N = 55
0
10
20
Kilometers
58°30'0"N
58°0'0"N
57°30'0"N
6°30'0"W
6°0'0"W
5°30'0"W
5°0'0"W

Fig. 1

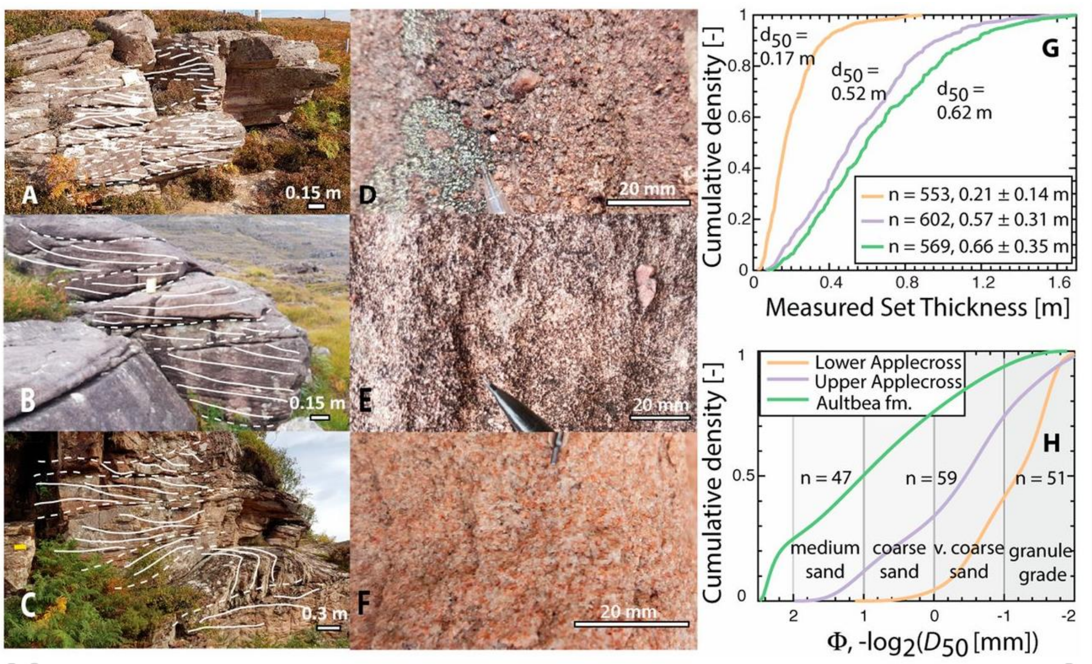
A
0.15 m
B
0.15 m
C
0.3 m
D
20 mm
E
20 mm
F
20 mm
G
Cumulative density [-]
Measured Set Thickness [m]
d50 = 0.17 m
d50 = 0.52 m
d50 = 0.62 m
n = 553, 0.21 ± 0.14 m
n = 602, 0.57 ± 0.31 m
n = 569, 0.66 ± 0.35 m
H
Lower Applecross
Upper Applecross
Aultbea fm.
n = 47
n = 59
n = 51
medium sand
coarse sand
v. coarse sand
granule grade
Φ, -log2(D50 [mm])

Fig. 2

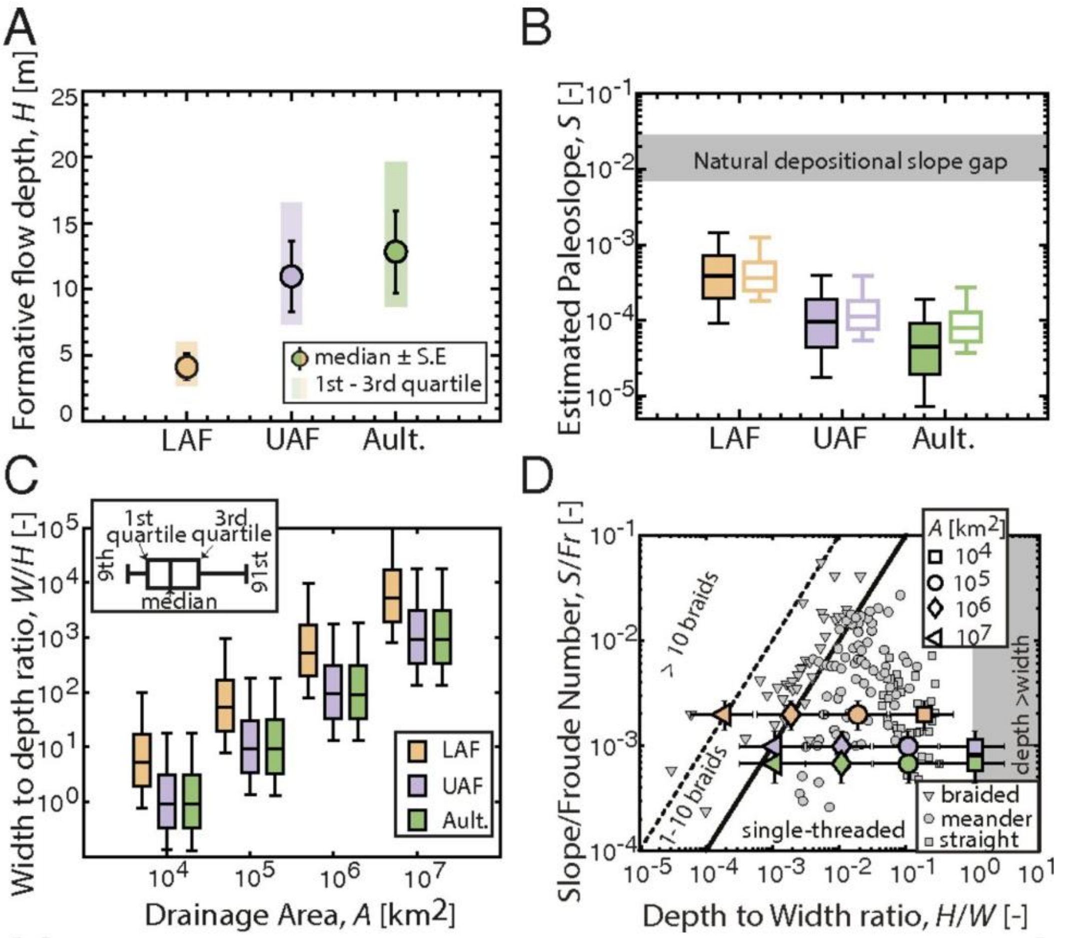
A
Formative flow depth, H [m]
median ± S.E
1st - 3rd quartile
LAF
UAF
Ault.
B
Estimated Paleoslope, S [-]
Natural depositional slope gap
LAF
UAF
Ault.
C
Width to depth ratio, W/H [-]
1st quartile
3rd quartile
9th
median
91st
LAF
UAF
Ault.
Drainage Area, A [km2]
D
Slope/Froude Number, S/Fr [-]
A [km2]
> 10 braids
1-10 braids
single-threaded
depth >width
braided
meander
straight
Depth to Width ratio, H/W [-]

Fig. 3

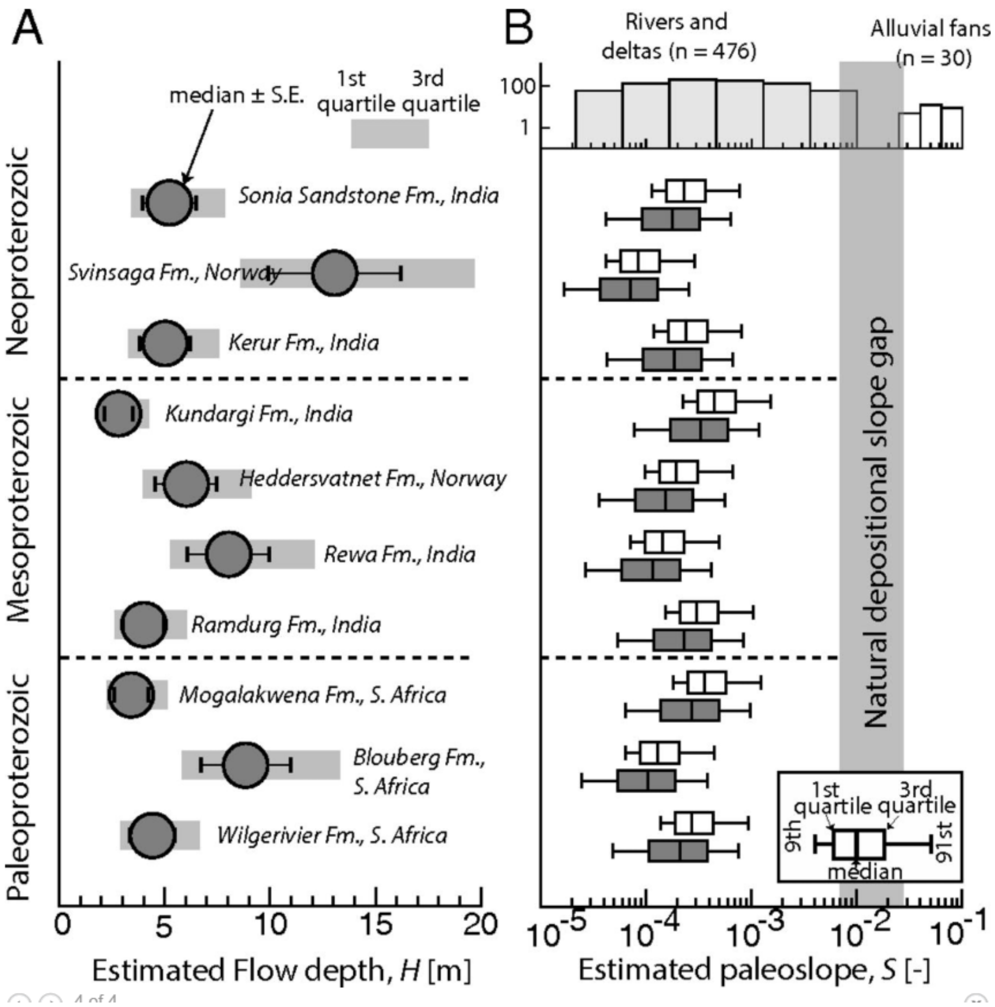

A
B
median ± S.E.
1st quartile
3rd quartile
Neoproterozoic
Mesoproterozoic
Paleoproterozoic
Sonia Sandstone Fm., India
Svinsaga Fm., Norway
Kerur Fm., India
Kundargi Fm., India
Heddersvatnet Fm., Norway
Rewa Fm., India
Ramdurg Fm., India
Mogalakwena Fm., S. Africa
Blouberg Fm., S. Africa
Wilgerivier Fm., S. Africa
0
5
10
15
20
Estimated Flow depth, H [m]
Rivers and deltas (n = 476)
Alluvial fans (n = 30)
100
1
Natural depositional slope gap
9th
91st
median
Estimated paleoslope, S [-]

Fig. 4

Supporting Information (SI Appendix): Low gradient, single-threaded rivers prior to greening of the continents

A. Geological Context and Regional Background

The “Torridonian Sandstone” is an informal stratigraphic name used to refer to the entire suite of Middle to Upper Proterozoic rocks exposed in the northwest highlands of Scotland, UK, comprising arkoses and subfeldspathic arenites, with occasional conglomerate and very minor shale horizons (1–4). They are internationally recognized as a classic type-example of Precambrian fluvial sedimentation. The rocks are exposed in a belt 20–30 km wide and more than 200 km long in northern Scotland (Fig. 1), lying underneath and cropping out in a window north of the trace of the regionally-significant Moine Thrust. They were deposited on top of Archean to Lower Proterozoic ‘Lewisian’ metamorphic basement over an unconformity surface with considerable erosional relief. Stratigraphically, the Torridonian succession has been divided into three groups (5): the Middle Proterozoic Stoer Group, the Sleat Group (which is mostly exposed on the Isle of Skye, Scotland, and whose relationship with the Stoer Group is enigmatic), and the Torridonian Group, which sits on an angular unconformity over the Stoer Group, but conformably overlies the Sleat Group where present. The data in this study solely refers to sedimentary strata of the Torridonian Group, which are Upper Proterozoic in age (4, 6). Diagenetic phosphate concretions in the lowest Torridonian Group yielded a whole rock Rb-Sr age of 994 ± 48 Ma and a Pb-Pb age of 951 ± 120 Ma (6, 7); these units unconformably overlie the well-studied Stac-Fada member of the Stoer Group, dated to 1177 ± 5 Ma (8), which constrains the onset of Torridonian sedimentation to early Neoproterozoic time. The Torridonian Group is unconformably capped by Cambrian quartzite (4).

B. Variability-dominated preservation of river dune evolution

Cross-stratified sets are depositional units formed by the migration of bedforms, and geometry of sets is controlled by the size of the formative bedforms, net aggradation rate, and the bedform celerity (9–12). Although the preservation of formsets can be common (12), especially when the local aggradation rates exceed bedform celerity, field evidence suggests that cross-stratification in the Torridonian Sandstone was a result of variable scours from migrating bedforms (Fig. S9). The empirical scaling relationship between cross-sets and formative bedform heights used in our study is based on an exact theory developed by Paola and Borgman (10) for the formation of cross-sets due to migrating bedforms under no net aggradation. They showed that the probability distribution of set thicknesses is given by the following one-parameter equation:

$$f(d_{st}) = \frac{ae^{-ad_{st}}\left(e^{-ad_{st}}+ad_{st}-1\right)}{\left(1-e^{-ad_{st}}\right)^2} \qquad \text{(S1)}$$

in which $d_{st} > 0$ is the set thickness, and a is the parameter of the distribution and is equal to $2/\beta$, where β is the scale parameter of the Gamma distribution describing the formative bedform heights. The theoretical coefficient of variation of the distribution of set thicknesses is 0.88 (10). The aforementioned distribution can be fit to the data when set thicknesses are measured at random spanning the entire set. Further, Bridge (13) demonstrated that the scaling relationship between cross-set thickness and mean bedform heights, and equation (S1) can be applied when the measured coefficient of variation of set thickness within a single set was 0.88 ± 0.3.

Measuring the set thickness across a complete set can be difficult in the field owing to the limited lateral exposure of outcrops; however, where near-complete exposure of sets were available in the field, the measured coefficient of variation of set thickness was within the bounds suggested by Bridge (13), and the theoretical density function of equation (S1) provided a reasonable description of the measured density of set thicknesses across the three stratigraphic intervals (Fig. S9). This observation is consistent with the inference that the bed sets were created by variables scours of migrating fluvial bedforms. Further, the estimated mean set thickness of these individual, near-complete sets was similar to the global mean of the set thickness within each stratigraphic interval. Thus, we used the global mean of set thickness within each stratigraphic interval for estimating the formative bedform heights.

C. Comparison of flow depth estimates using different scaling relationships

Several studies have demonstrated that bedform heights can be related to their formative flow depth, transport stage, grain size, shear stress and other parameters of the flow conditions (14); however, not all these relationships can be used within a stratigraphic framework owing to the difficulty of robust inversion of key parameters of flow conditions. In this study, we used the h_d-H scaling relation reported by Bradley and Venditti (14). Other commonly used scaling relationships to invert for H include a relation provided by Leclair and Bridge (9), which builds on the work of Yalin (15), where the ratio of H to h_d was constrained to lie within a range of 6 to 10 with a mean of 8. Allen (16) provided a different formula for estimating H given by:

$$H = 11.62(h_d)^{0.84} \quad \text{(S2)}$$

where all quantities are in m. Estimating the formative flow depths from the aforementioned methods did not change our results significantly (Fig. S12). We used the method presented in Bradley and Venditti (14) because the uncertainty in the prediction of H was constrained, which allowed us to propagate this uncertainty into the estimation of slope and aspect ratio of channels through Monte Carlo sampling.

D. Bedform stability diagrams

Several decades of experimental and field research resulted in the formulation of a graphical framework that represents the conditions of flow, sediment transport, and fluid properties necessary for the stable existence of various bed states in alluvial rivers (e.g., ripples, dunes, lower plane bed, upper plane bed, antidunes)(17–22). Dimensional analysis indicates that at least three independent dimensionless numbers are required to characterize the stability of bedform states, and the commonly used dimensionless numbers are Froude number (*Fr,* which determines the state of the flow), Shields parameter (τ^*, describes the intensity of sediment transport), and particle Reynolds number (Re_p, that accounts for grain size and fluid viscosity), given by:

$$Fr = \frac{U}{\sqrt{gH}} \qquad \text{(S3a)}$$

$$\tau^* = \frac{\tau_b}{(\rho_s - \rho) g D_{50}} \qquad \text{(S3b)}$$

$$Re_p = \frac{\sqrt{R g D_{50}^3}}{\nu} \quad \text{(S3c)}$$

where U is the depth-averaged flow velocity, g is the gravitational acceleration, H is the flow depth, τ_b is the bed shear stress approximated as ρgHS for steady, uniform flow conditions, ρ_s is the density of sediment, ρ is the density of fluid, D_{50} is the median grain-size, R is the submerged specific density of sediment, and ν is the kinematic viscosity of the fluid, which is temperature-dependent. For subcritical flows, the bedform stability diagram is independent of the Froude number and can be expressed in terms of the Shields stress and the particle Reynolds number. We used the bedform stability diagram of Lamb et al. (19) to constrain the dimensionless bed shear stress in this study. Lamb et al. (19) compiled existing field and experimental studies, and constructed a comprehensive bedform stability diagram that spans a large range in particle Reynolds numbers. Using this compilation, they delineated the boundaries between different bed states (Fig. S10A). We estimated the particle Reynolds number for our stratigraphic sampling intervals using the measured median grain-size (Fig. 2H), and by assuming a kinematic viscosity of water of 10^{-6} m^2/s. Froude number, which is needed for evaluating the stability of planform morphology (Fig. 3D), was estimated for Torridonian rivers using equation (S3a).

E. Data compilation of Proterozoic cross-set thickness

We compiled cross-set thickness across 10 fluvial formations in the Proterozoic Eon (23–29). We chose a representative global sample that spanned Paleoproterozoic to Neoproterozoic deposits and restricted our compilation to studies that made extensive measurements of cross-set thickness to ensure that the measurements were a representative sample of each formation. Median grain-size measurements were not directly reported in previous studies; however, they noted that the cross-sets were composed of medium-to-coarse sand. In some cases, we corroborated these estimates using the reported microphotographs of the sandstone units. For each formation, we estimated paleoslope by taking a conservative approach, where we assumed the median grain-size to be uniformly distributed and bound by 0.5 to 1.5 mm for Monte Carlo sampling (equations 2, 3 in *Materials and Methods*). Similar to the paleohydraulic analyses of the Torridonian Group, we estimated the flow depth from H-h_d scaling relation (equation 1 in *Materials and Methods*) and we used both the bedform stability diagram and modern empirical scaling relationships to estimate paleoslope through Monte Carlo sampling (Fig. 4 in main text).

F. Previous estimates of paleogradients of Proterozoic rivers

A range of studies spanning three Paleoproterozoic formations, two Mesoproterozoic formations and multiple Neoproterozoic formations across four continents have suggested that gradients of Proterozoic rivers were steeper than that observed in post-Cambrian systems (23, 24, 26, 30–35). These studies estimated gradients using measured cross-stratal thickness and empirical relationships based on width-depth scaling and discharge-width scaling of modern rivers. In particular, all these studies used empirical relationships that relate paleoslope to the width-depth ratio of flows and percentage of silt and clay in the channel perimeter (36, 37). Width-depth ratios were also empirically related to the percentage of silt and clay in the channel perimeter, which was equated to 5% on the basis of the *a priori* assumption that Proterozoic rivers were large bedload systems that were devoid of any cohesive bank strength. These results yielded average slopes for Proterozoic rivers that spanned 4×10^{-3} to 4×10^{-2}. These observations suggest that Proterozoic rivers resided in the natural depositional slope gap between modern alluvial fans and rivers — a consequence of hydrodynamic differences between flows (Froude-supercritical vs Froude-subcritical) that shape alluvial fans and rivers, respectively (38). Consensus on the cause of steep Proterozoic fluvial gradients is currently lacking, and previous studies have attributed this inference to unique combination of weathering regime in the Proterozoic Eon and lack of vegetation (24), tectono-sedimentary history of basin evolution in combination with rigorous climate (33), and production of argillaceous sediment under hyper-greenhouse atmospheric conditions, which enabled temporary storage of this sediment to sustain steep slopes (26). It has also been noted that none of these mechanisms provide a unifying explanation for the steep fluvial gradients inferred in Proterozoic deposits worldwide, given that mud preservation in most Proterozoic fluvial systems is negligible (23). The lack of consensus on the cause of steep gradients across Proterozoic rivers together with the geodynamical implications indicated in our study suggest that steep super-continental-scale Proterozoic rivers that resided in the natural depositional slope gap between alluvial fans and alluvial rivers were unlikely to have existed. Moreover, the inferred steep paleoslopes from previous studies are inconsistent with the observation of ubiquitous cross-stratification throughout the Proterozoic eon, and also with the inference that these rivers represented predominantly bedload systems.

G. Data compilation of modern rivers

We compiled 476 modern fluvial gradients (38–42), in addition to 30 modern alluvial fan gradients (38). Figure 4B in the main text shows the histograms of the fluvial gradients measured in modern rivers and alluvial fans along with the hypothesized natural depositional slope gap (38). In Figure 3D of the main text, we reproduced the ratio of slope and Froude number and the depth to width ratios reported in Parker (43) for modern braided, meandering, and straight channels.

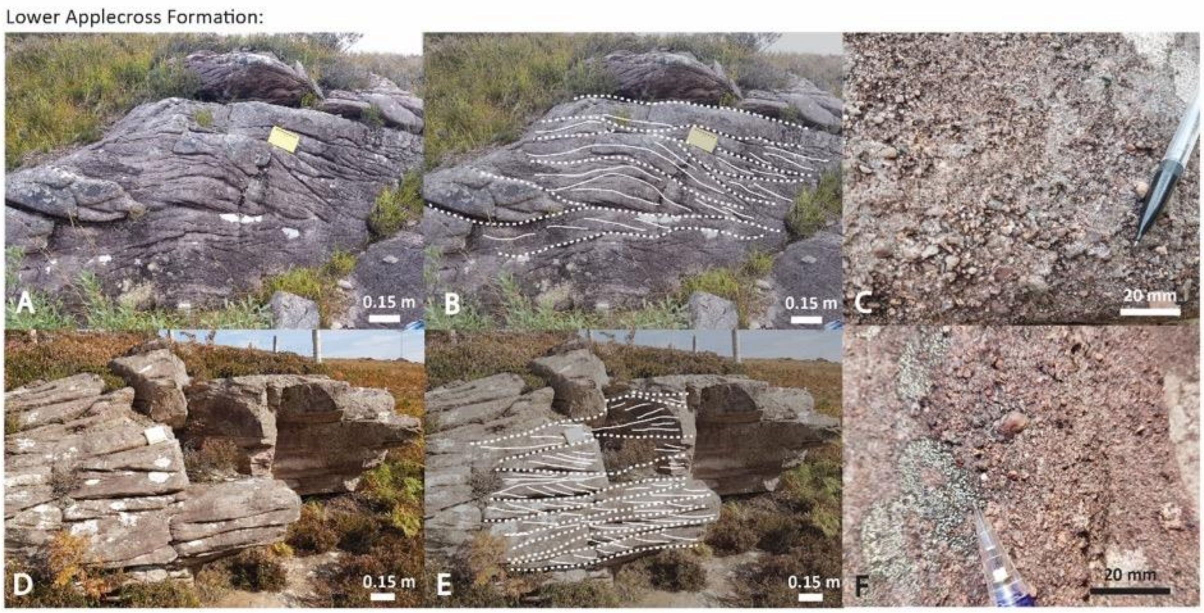

Fig. S1. Supplementary field photographs in the Lower Applecross. A, D) Original field photographs in the Lower Applecross. B, E) Annotated images where the dashed lines indicate the interpreted erosional boundaries and the solid lines indicate the observed cross-bedding. C, F) Representative macro photographs showing the grain-size observed at individual outcrops.

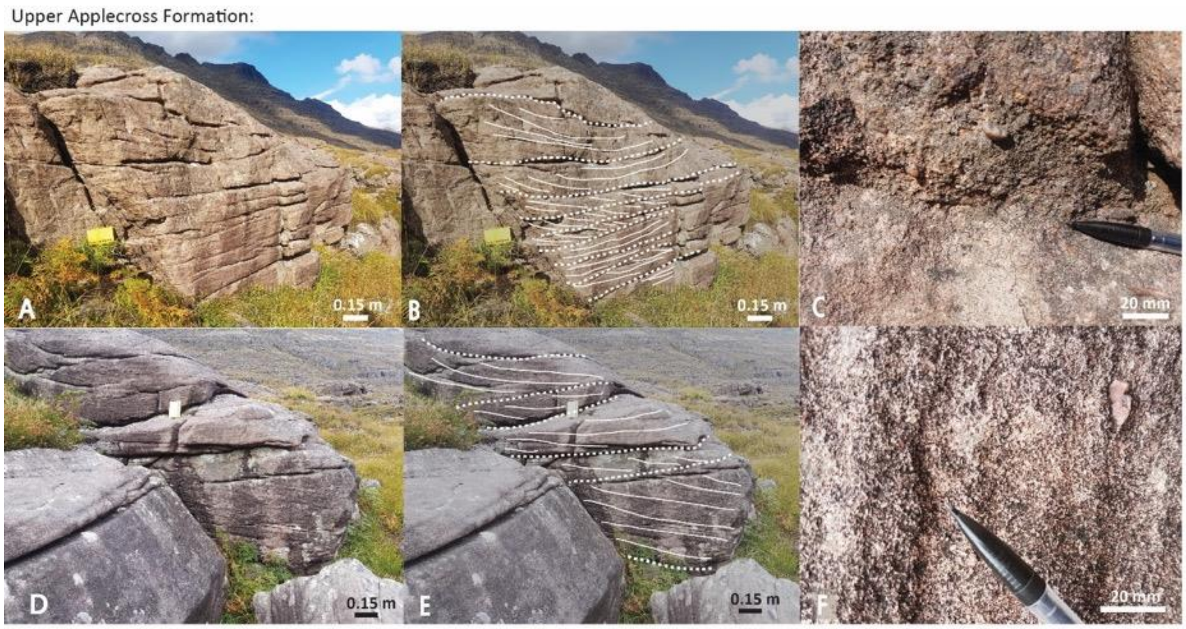

Fig. S2. Supplementary field photographs in the Upper Applecross. A, D) Original field photographs in the Upper Applecross. B, E) Annotated images where the dashed lines indicate the interpreted erosional boundaries and the solid lines indicate the observed cross-bedding. C, F) Representative macro photographs showing the grain-size observed at individual outcrops.

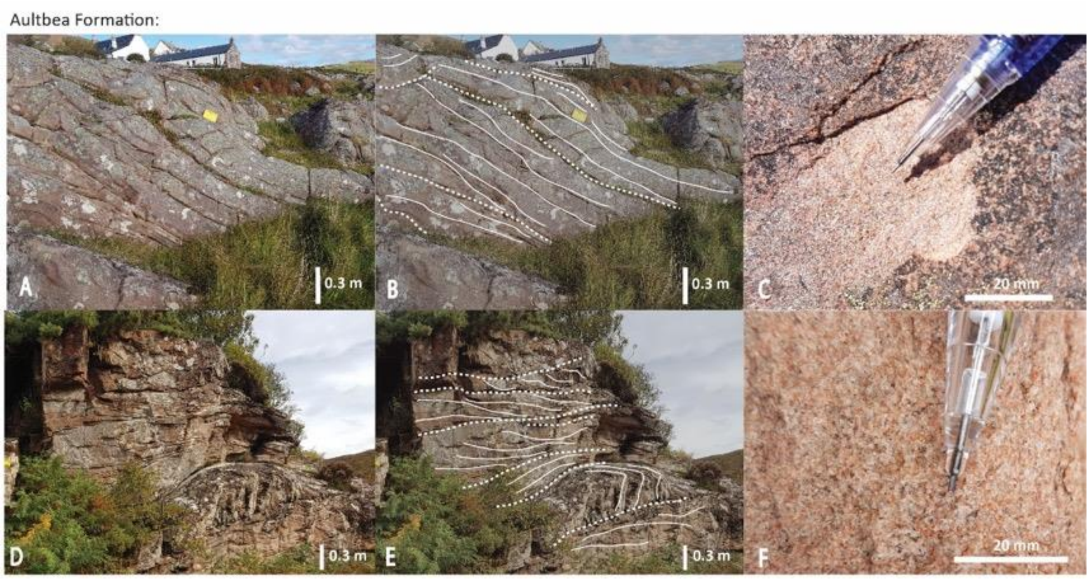

Fig. S3. Supplementary field photographs in the Aultbea Formation. A, D) Original field photographs in the Aultbea Formation. B, E) Annotated images where the dashed lines indicate the interpreted erosional boundaries and the solid lines indicate the observed cross-bedding. C, F) Representative macro photographs showing the grain-size observed at individual outcrops.

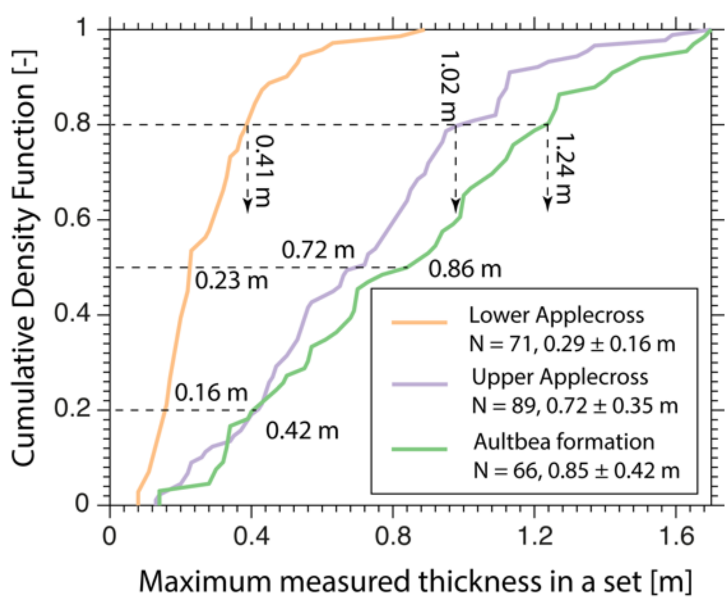

Fig. S4. Maximum set thickness measured within individual sets. Cumulative density function of the maximum set thickness measured within individual sets across the three stratigraphic sampling intervals. The dashed lines indicate 20th, 50th, and 80th percentile of the maximum set thickness. The mean and standard deviation of the maximum set thickness is indicated in the figure legend. The increase in set thickness with stratigraphic height is evident not only in the bulk statistics of set thickness (Fig. 2G), but also in the measured maximum set thickness within individual sets across LAF, UAF, and Aultbea Formation.

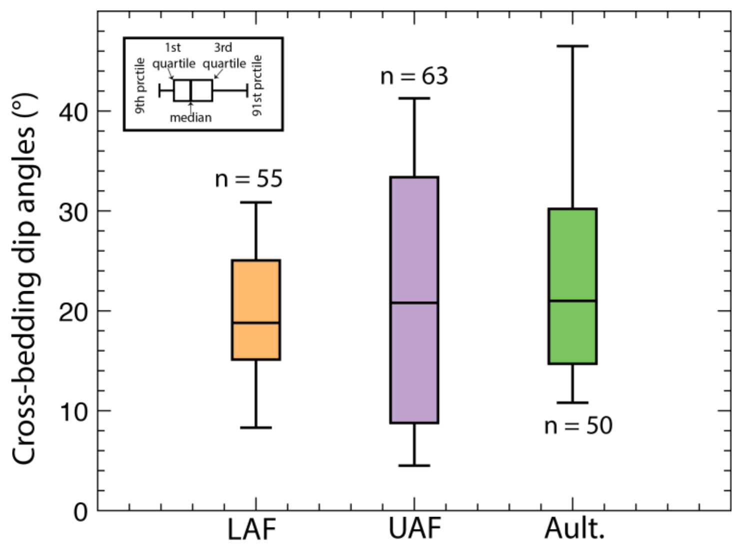

Fig. S5. Cross-bedding angles measured in the Torridonian Group. Boxplots of the measured cross-bedding angles, which were corrected for the depositional dip (orange – LAF; purple – UAF; green – Aultbea Formation). These dip angles are similar to modern lee-face angles of river dunes, and markedly shallower than the dip of the inferred lateral accretion surfaces (Figs. S6, S7).

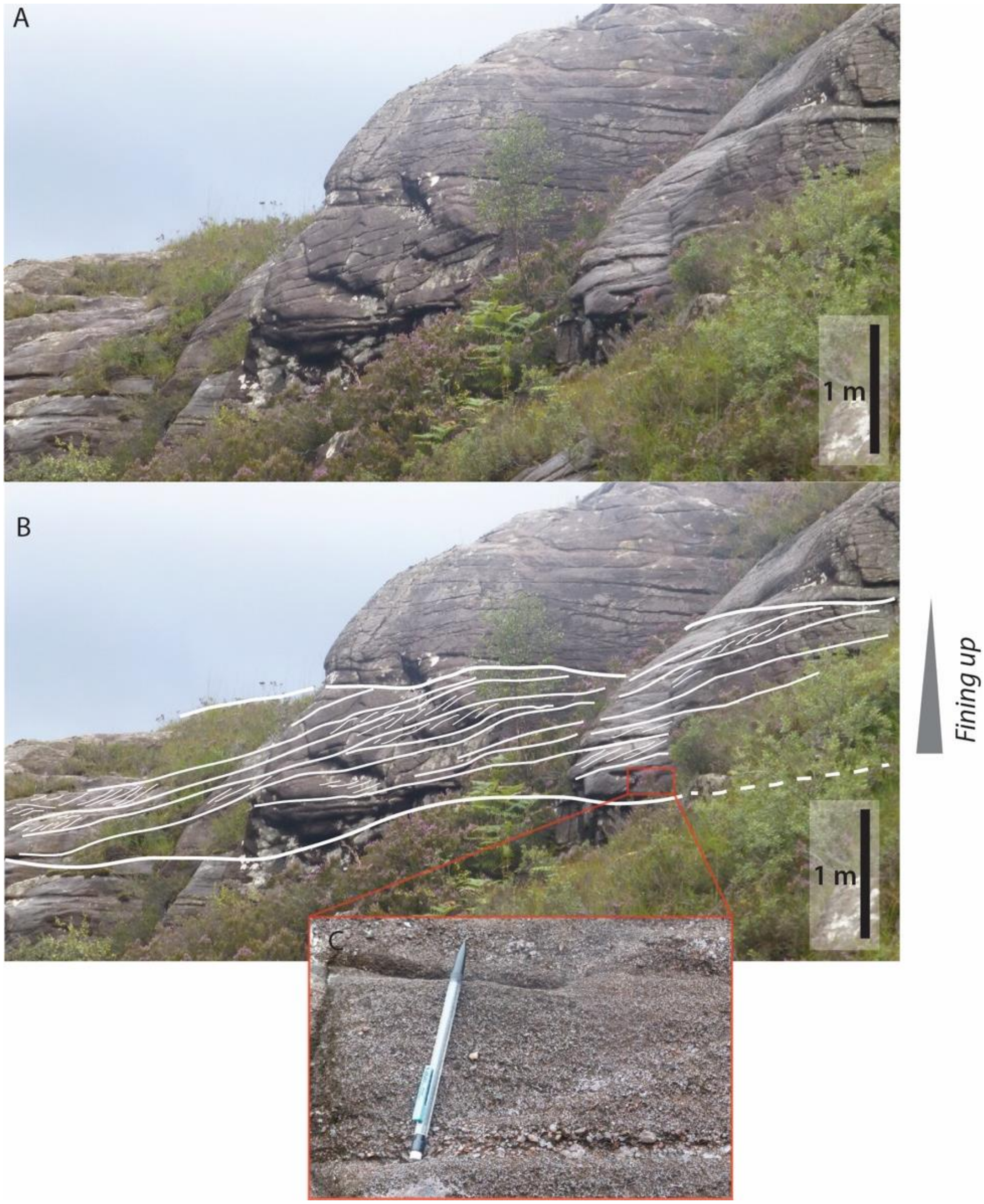
A
1 m
B
Fining up
1 m
C

Fig. S6. Rare preserved barform in the Lower Applecross. A) Uninterpreted and B) interpreted truncated barform outcrop photographs in the Lower Applecross (location coordinates: NG 95500 68702). The deposits are characterized by upward fining with the base of the major erosional surface composed of pebble lag (C). This coarse pebble lag is also a feature of the major erosional surface that bound the inferred lateral accretion sets. Solid, thick white lines indicate the lateral accretion surfaces and thin white lines indicate cross-stratification, which was inferred to represent superimposed bedforms on this putative barform. The maximum measured thickness of this truncated barform was 1.7 m.

Fig. S7. Rare preserved barform in the Upper Applecross. A) Uninterpreted and B) interpreted truncated barform outcrop photographs in the Upper Applecross (location coordinates: NG 91694 55653). Solid, thick white lines indicate the lateral accretion surfaces and thin white lines indicate cross-stratification, which was inferred to represent superimposed bedforms on this putative barform. The maximum measured thickness of this truncated barform was 4.7 m.

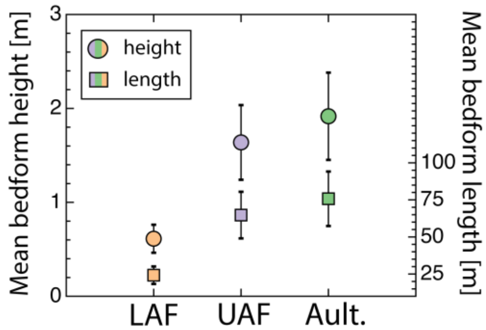

Fig. S8. Reconstructed geometry of bedforms in the Torridonian Sandstone. Reconstructed bedform heights using scaling of mean cross-set thickness and formative dune heights (left axis; circular markers). The bedform lengths were reconstructed using the empirical scaling relationship presented in Bradley and Venditti (14) (right axis; square markers).

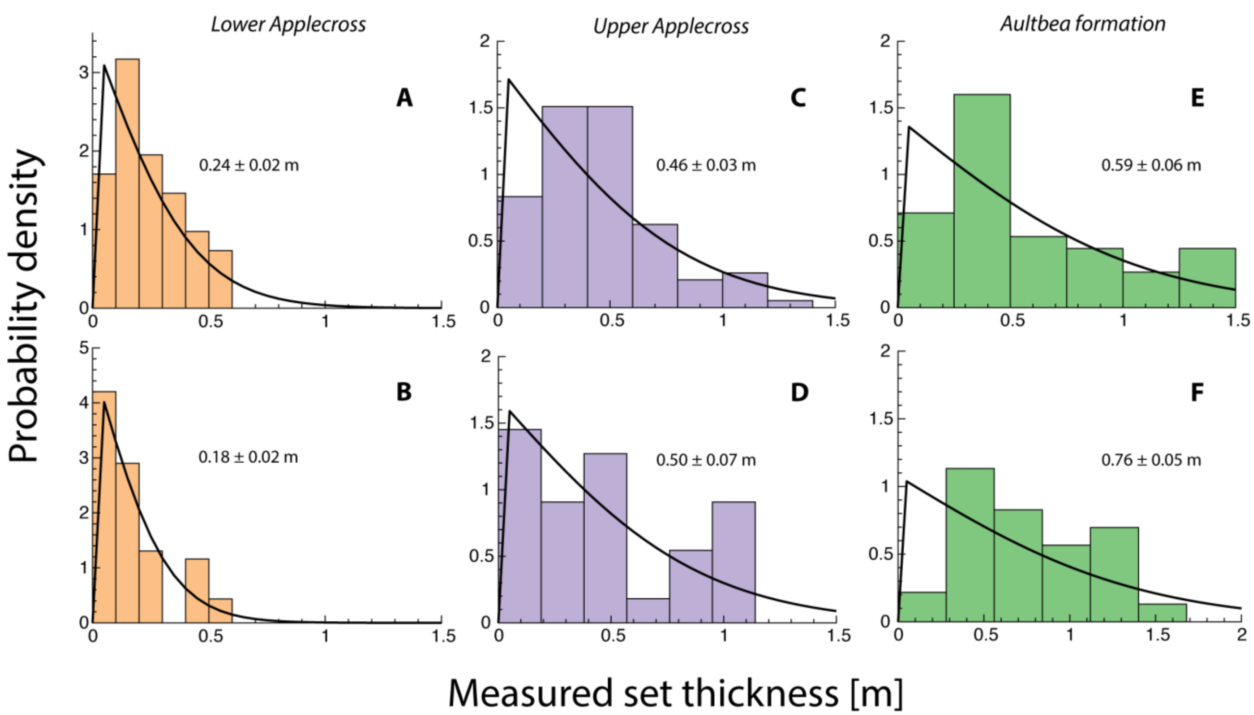

Fig. S9. Comparison of set thickness distribution with theory. Estimated probability density functions for measured set thicknesses where near-complete exposure of sets was available for (A-B) Lower Applecross, (C-D) Upper Applecross, and (E-F) Aultbea Formation. The solid black lines indicate the theoretical prediction (10) where the parameter *a* was estimated using $a = 1.64493/\langle d_{st} \rangle$.

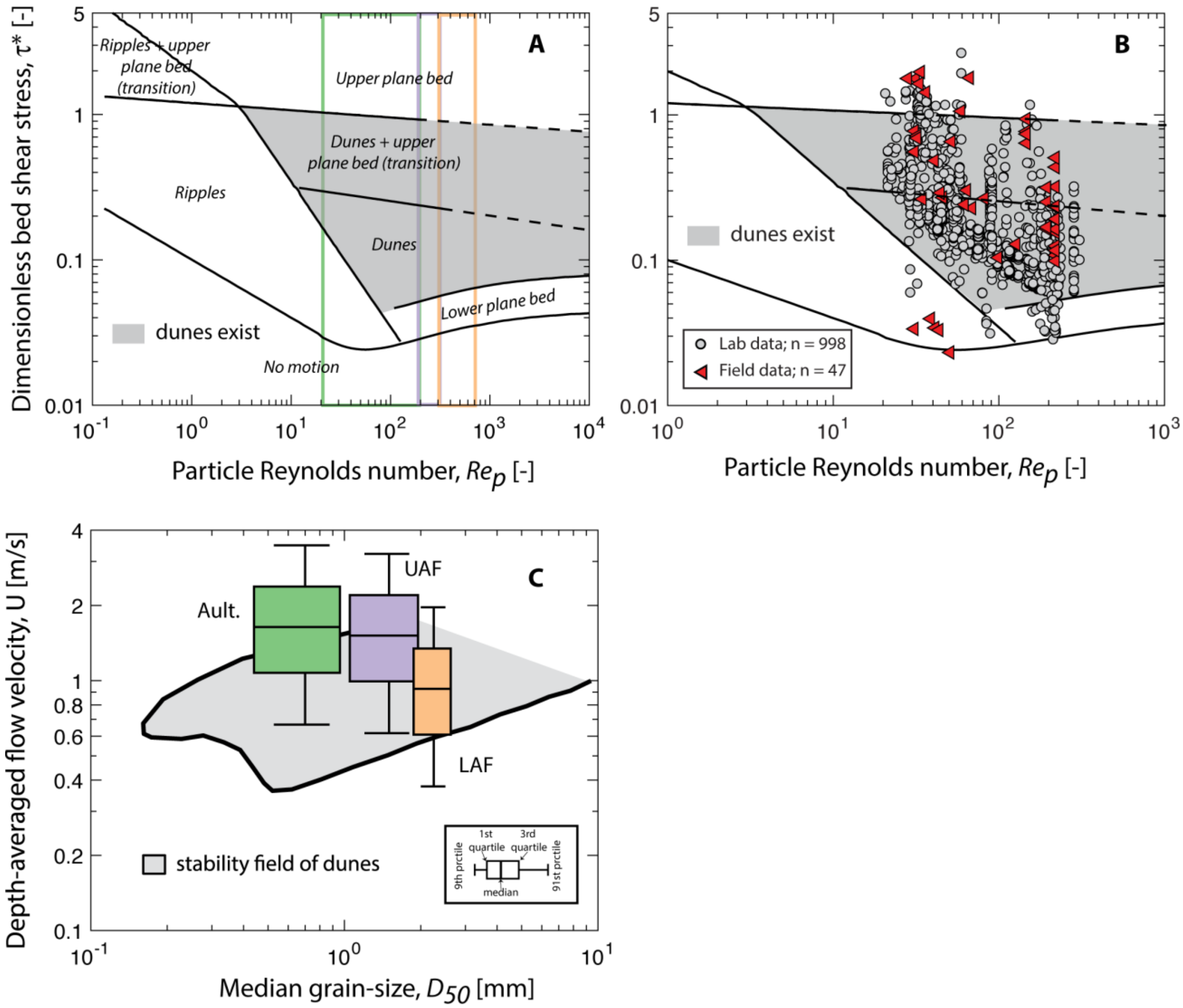

Fig. S10. Bedform stability diagram. A) Bedform stability diagram of Lamb et al. (19). The highlighted gray area indicates the stability field for the existence of river dunes. The estimated particle Reynolds number (equation S3C) for the three stratigraphic sampling intervals are indicated using colored rectangles. The solid black lines are fits of Lamb et al. (19) to the bedform transition boundaries validated using existing experimental or field studies. The dashed black lines denote the extrapolation of these bedform transition boundaries to higher particle

Reynolds numbers (19). B) Laboratory and field data with the same Re_p range as the Torridonian Sandstone. The solid gray markers are experimental data, and the red triangles are field data, which were derived from a recent global compilation (20). C) Bedform stability diagram expressed in terms of depth-averaged flow velocity and median grain-size (18), where the region bounded by the solid black line delineates the phase space for the stable existence of fluvial dunes. Estimated depth-averaged flow velocities using Monte Carlo sampling are also indicated (equation 5 in *Materials and Methods*).

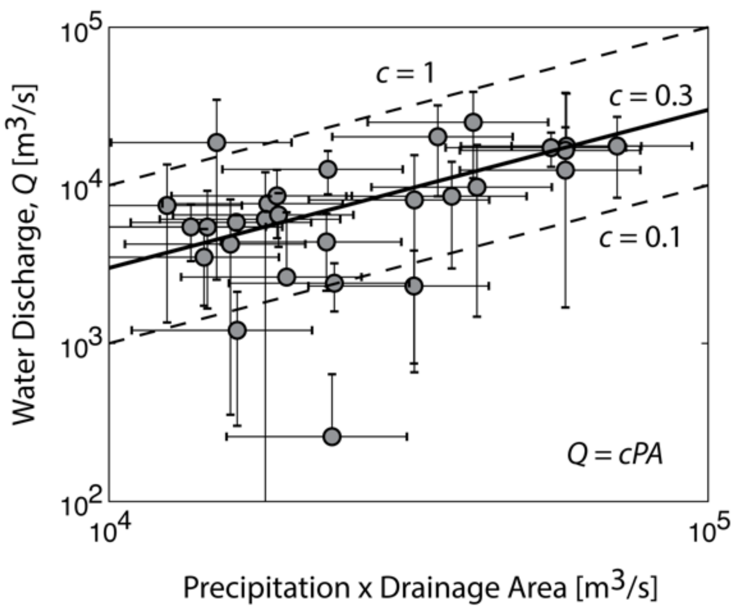

Fig. S11. Relationship between water discharge, precipitation rate, and drainage area in modern continental-scale rivers in subtropical and temperate regions. The mean and standard deviation of the observed water discharge are shown on the y-axis. The average period of record varies from station to station with a mean of 21.5 years (44). The product of monthly precipitation rate and drainage area are indicated on the y-axis. The markers indicate the computed value of *PA* for *P* = 0.75 m/yr, and the error bars show the extent of computed value for *P* = 0.5 m/yr and 1 m/yr.

This range corresponds to the observed global mean monthly precipitation rates in the subtropical and temperate regions (45).

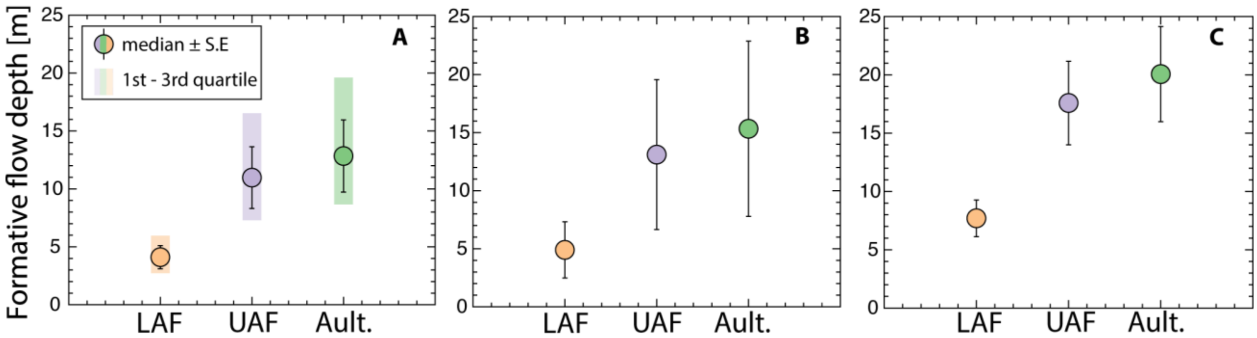

Fig. S12. Estimated flow depths for the Torridonian Group. A) Estimated *H* using the scaling relationship and the uncertainties of (14). B) Estimated *H* using the values of H/h_d reported in (9). C) Estimated *H* using equation (S2) proposed by Allen (16).

Table S1. Cross-set thickness and median grain-size measured in the Torridonian Group

Coordinates	Stratigraphic sampling interval	Mean cross-set thickness [m]	Number of measurements	Estimated median grain-size [mm]	Additional notes
NG 93150 78407	LAF	0.22	57	2.5; 1.5	7 sets observed. Bottom set was v. coarse sand to granules, and top 6 sets were coarse to v. coarse sand
NG 92715 70420	LAF	0.17	80	2.0; 3.0; 4.0	11 sets observed. Granules were typical of most sets. One set composed of fine gravel, and one set composed of granules

NG 76853 73710	LAF	0.14	97	2.0; 3.0	12 sets identified. All deposits were characterized by granules with some sets coarser with granules between 2 to 4 mm.
NG 79192 - 60530	LAF	0.66	10	2.0	v. coarse sand to granules
NC 22492 - 24866	LAF	0.24	41	1.5; 3.0; 0.8	bottom 3 sets were v. coarse sand, and one set was composed of granules. Top set was composed to medium to coarse sand
NC 22545 - 24814	LAF	0.17	69	1.5	v. coarse sand
NC 22552 - 24746	LAF	0.15	70	3.0; 2.5; 1.5	3 sets with overall upward fining trend. The grain size in sets ranged from granules and occasional pebbles to v. coarse sand

NC 15426 - 05634	LAF	0.41	26	2.5; 3.0; 2.5; 3.0; 2.5	v. coarse sand to granules with occasional pebbles
NC 15436 - 05600	LAF	0.26	57	2.5; 3.0; 2.5; 3.0; 2.5	v. coarse sand to granules with occasional pebbles
NG 95806 68529	LAF	0.28	12	3.0; 2.0; 1.5	3 sets with upward fining trend. Granules in bottom set and v. coarse sand in the top set
NG 95565 68685	LAF	0.23	8	1.0	Coarse sand
NG 95500 68702	LAF	0.22	10	1.0	Coarse sand
NG 95463 68727	LAF	0.27	7	1.3; 2.5	Stratigraphically higher set had 1 to 2 mm sediment sizes visible, but dominantly made up of sediment size close to 1 mm.

					Lowest set was composed of granules in the 2 to 3 mm range.
NG 95178 68806	LAF	0.26	9	1.5	Dominantly 1 to 2 mm with granules at the base of sets.
NG 77774 - 41846	UAF	0.70	9	1	Medium to coarse sand with grain size closer to 1 mm
NG 77778 - 41705	UAF	0.44	6	0.75	Observed grain size was between 0.5 and 1 mm
NG 77779 - 41641	UAF	0.84	11	0.5	Medium to coarse sand
NG 77727 - 41579	UAF	0.46	28	0.4	Medium sand and slightly finer than previous location
NG 77922 - 41565	UAF	0.67	15	0.4	Medium sand and slightly finer than NG 77779-41641 location sets

NG 91678 55533	UAF	0.80	42	2.5; 1.5; 0.75	6 sets were observed. Bottom set was v. coarse sand with pebbles. Higher 3 sets were coarse to v. coarse sand. The top 2 sets were medium to coarse sand, finer than 1 mm but coarser than 0.5 mm
NG 91653 55704	UAF	0.78	36	1.75; 1.5; 1	4 sets observed. The middle set was v.coarse sand. The bottom set was coarser than the middle set but still v. coarse sand. The top sets were coarse to v. coarse sand.

NG 91921 55947	UAF	0.79	25	0.75; 0.5; 1.5; 2	4 sets were interpreted with different grain-sizes. The sets were composed of v. coarse sand with pebbles, coarse to v. coarse sand, medium to coarse sand, and coarse to v. coarse sand
NG 91942 55960	UAF	0.42	30	2.5	5 sets were observed and all sets were composed of pebbles and coarse granules
NG 91901 55936	UAF	0.71	41	1; 0.5; 2.5; 1; 1; 1.5	6 sets observed with varying grain-sizes. We noted sets with coarse sand with some pebbles, medium to coarse sand, granules, and coarse sand

NG 91701 55534	UAF	0.49	29	3; 1.5; 1.5; 1.5; 2.5	5 sets were observed. One set was composed of granules, another set was composed of coarse to v. coarse sand with lenses of medium sand. Two sets were classified as v. coarse sand, and finally one set was v. coarse sand with granules > 2 mm.
NG 76832 43318	UAF	0.97	20	0.5	All 3 sets composed of medium sand
NG 76796 43296	UAF	0.42	30	0.5; 1; 2	4 sets observed with 2 sets composed of medium sand, one set composed of coarse sand and one set composed of v. coarse sand and pebbles

NB 98096 12863	UAF	0.45	96	1.5	8 sets observed and all composed of v. coarse sand
NB 97224 13317	UAF	0.52	39	1.5; 3.5; 3; 4	5 sets observed, which were much coarser than other UAF sets. Pebbles and granules were noted throughout the locality
NG 84374 91884	UAF	0.49	82	1.5	9 sets observed. All sets composed of v. coarse sand with occasional granules and pebbles
NG 84022 92369	UAF	0.40	63	1.5; 3; 1.5	8 sets were observed. All sets were composed of v. coarse sand except for one. That set was composed of granules and very fine gravel
NG 71230 39983	Ault.	0.79	48	0.5	Medium sand in all sets. 4 sets were observed

NG 71314 39873	Ault.	0.72	33	0.2	Fine to medium sand
NG 71024 37955	Ault.	0.58	45	0.2	5 sets composed of fine to medium sand
NG 71210 38192	Ault.	0.69	22	0.35	3 sets were identified.
NG 71024 37955	Ault.	0.43	32	0.2	Fine to medium sand
NG 71172 38779	Ault.	0.62	19	0.2	Fine to medium sand
NG 88706 94043	Ault.	0.45	31	0.2	Fine to medium sand
NG 88663 94099	Ault.	0.51	27	0.75; 1.25	3 sets were identified, and they were composed of medium to coarse sand, and coarse to v. coarse sand
NG 88774 94062	Ault.	0.62	36	0.75; 1; 0.2	4 sets were identified, and they were composed of coarse sand, and fine to medium sand

NB 98947 13842	Ault.	0.76	82	0.75; 0.2	9 sets were identified. 3 of them were composed of coarse sand, and the rest were composed of fine to medium sand
NB 99315 10309	Ault.	0.58	48	0.5	Medium sand
NB 99050 09933	Ault.	0.93	43	0.5	Medium sand
NG 88934 95450	Ault.	0.87	50	0.5; 0.25	Total of 4 sets were identified. 3 sets composed of medium sand, and one set composed of fine to medium sand
NG 85160 - 90783	Ault.	0.12	9	1.5; 2.5	Only instance in Aultbea formation where granules > 2 mm were documented
NG 89150 - 96078	Ault.	0.49	20	1.5	3 v. coarse sand sets

NG 89169-960568	Ault.	0.46	13	1; 1.5	Sets with coarse sand and v. coarse sand were documented
NG 89202 - 96095	Ault.	0.68	11	1; 1.5	v. coarse sand with occasional pebble/granule

Supplementary References

1. Peach BN, Horne J (1892) The Olennellus Zone in the north-west Highlands of Scotland. *Q J Geol Soc* 48(1888):227–242.
2. Allen P (1948) Wealden petrology : The Top Ashdown Pebble Bed and the Top Ashdown Sandstone. *Q J Geol Soc* 104(1–4):257 LP-321.
3. Nicholson PG (1993) *A basin reappraisal of the Proterozoic Torridon Group, northwest Scotland* (International Association of Sedimentologists).
4. Stewart AD (2002) The later Proterozoic Torridonian rocks of Scotland: their sedimentology, geochemistry and origin. *Geological Society, London* (Geological Society of London), p 132.
5. Stewart AD (1969) Torridonian Rocks of Scotland Reviewed. *AAPG, Memoirs*, ed Kay M (American Association of Petroleum Geologists), pp 595–608.
6. Kinnaird TC, et al. (2007) The late Mesoproterozoic–early Neoproterozoic tectonostratigraphic evolution of NW Scotland: the Torridonian revisited. *J Geol Soc London* 164(3):541–551.
7. Turnbull MJM, Whitehouse MJ, Moorbath S (1996) New isotopic age determinations for the Torridonian, NW Scotland. *J Geol Soc London* 153(6):955–964.
8. Parnell J, Mark D, Fallick AE, Boyce A, Thackrey S (2011) The age of the Mesoproterozoic Stoer Group sedimentary and impact deposits, NW Scotland. *J Geol Soc London* 168(2):349–358.
9. Leclair SF, Bridge JS (2001) Quantitative Interpretation of Sedimentary Structures Formed by River Dunes. *J Sediment Res* 71(5):713–716.
10. Paola C, Borgman L (1991) Reconstructing random topography from preserved stratification. *Sedimentology* 38(4):553–565.
11. Ganti V, Paola C, Foufoula-Georgiou E, Foufoula-Georgiou E (2013) Kinematic controls on the geometry of the preserved cross sets. *J Geophys Res Earth Surf* 118(3):1296–1307.
12. Reesink AJHH, et al. (2015) Extremes in dune preservation: Controls on the completeness of fluvial deposits. *Earth-Science Rev* 150:652–665.
13. Bridge JS (1997) Thickness of sets of cross strata and planar strata as a function of formative bed-wave geometry and migration, and aggradation rate. *Geology* 25(11):971–974.
14. Bradley RW, Venditti JG (2017) Reevaluating dune scaling relations. *Earth-Science Rev* 165:356–376.
15. Yalin MS (1964) Geometrical properties of sand waves. *J Hydraul Div* 90(5):105–119.
16. Allen JRL (1968) *Current Ripples* (North-Holland Publishing Co., Amsterdam).
17. Southard JB, Boguchwal LA (1990) Bed configuration in steady unidirectional water flows; Part 2, Synthesis of flume data. *J Sediment Res* 60(5):658–679.
18. Carling PA (1999) Subaqueous gravel dunes. *J Sediment Res* 69(3):534–545.

19. Lamb MP, Grotzinger JP, Southard JB, Tosca NJ (2012) Were Aqueous Ripples on Mars Formed by Flowing Brines? *Sedimentary Geology of Mars*, eds Grotzinger JP, Milliken RE (SEPM Society for Sedimentary Geology). Available at: https://doi.org/10.2110/pec.12.102.0139.
20. Ohata K, Naruse H, Yokokawa M, Viparelli E (2017) New Bedform Phase Diagrams and Discriminant Functions for Formative Conditions of Bedforms in Open-Channel Flows. *J Geophys Res Earth Surf* 122(11):2139–2158.
21. Allen JRL (1984) *Sedimentary Structures; Their Character and Physical Basis* (Elsevier, Amsterdam).
22. Southard JB (1991) Experimental Determination of Bed-Form Stability. *Annu Rev Earth Planet Sci* 19(1):423–455.
23. Mukhopadhyay S, Choudhuri A, Samanta P, Sarkar S, Bose PK (2014) Were the hydraulic parameters of Precambrian rivers different? *J Asian Earth Sci* 91:289–297.
24. Van der Neut M, Eriksson PG (1999) Palaeohydrological parameters of a Proterozoic braided fluvial system (Wilgerivier Formation, Waterberg Group, South Africa) compared with a Phanerozoic example. *IAS Spec Publ* 28:381–392.
25. Eriksson PG, Bumby AJ, Brümer JJ, van der Neut M (2006) Precambrian fluvial deposits: Enigmatic palaeohydrological data from the c. 2–1.9 Ga Waterberg Group, South Africa. *Sediment Geol* 190(1):25–46.
26. Eriksson P, et al. (2008) Palaeohydrological data from the c. 2.0 to 1.8 Ga Waterberg Group, South Africa: discussion of a possibly unique Palaeoproterozoic fluvial style. *South African J Geol* 111(2–3):281–304.
27. Köykkä J (2011) Precambrian alluvial fan and braidplain sedimentation patterns: Example from the Mesoproterozoic Rjukan Rift Basin, southern Norway. *Sediment Geol* 234(1–4):89–108.
28. Köykkä J (2011) The sedimentation and paleohydrology of the Mesoproterozoic stream deposits in a strike-slip basin (Svinsaga Formation), Telemark, southern Norway. *Sediment Geol* 236(3–4):239–255.
29. Sarkar S, Samanta P, Mukhopadhyay S, Bose PK (2012) Stratigraphic architecture of the Sonia Fluvial interval, India in its Precambrian context. *Precambrian Res* 214–215:210–226.
30. Eriksson PG, Bose PK, Catuneanu O, Sarkar S, Banerjee S (2008) Precambrian clastic epeiric embayments: examples from South Africa and India. *Dyn epeiric seas* 48:119–136.
31. Rainbird RH (1992) Anatomy of a large-scale braid-plain quartzarenite from the Neoproterozoic Shaler Group, Victoria Island, Northwest Territories, Canada. *Can J Earth Sci* 29(12):2537–2550.
32. Köykkä J (2011) Precambrian alluvial fan and braidplain sedimentation patterns: Example from the Mesoproterozoic Rjukan Rift Basin, southern Norway. *Sediment Geol* 234(1–4):89–108.
33. Köykkä J (2011) The sedimentation and paleohydrology of the Mesoproterozoic stream deposits in a strike-slip basin (Svinsaga Formation), Telemark, southern Norway. *Sediment Geol* 236(3–4):239–255.
34. Sarkar S, Samanta P, Mukhopadhyay S, Bose PK (2012) Stratigraphic architecture of the Sonia Fluvial interval, India in its Precambrian context. *Precambrian Res* 214–215:210–226.
35. Eriksson PG, Bumby AJ, Brümer JJ, van der Neut M (2006) Precambrian fluvial deposits: Enigmatic palaeohydrological data from the c. 2–1.9 Ga Waterberg Group, South Africa. *Sediment Geol* 190(1):25–46.
36. Schumm SA (1968) *River Adjustment to Altered Hydrologic Regimen- Murrumbidgee River and Paleochannels, Australia* (US Government Printing Office).
37. Schumm SA (1972) Fluvial Paleochannels. *Sepm*, eds Rigby JK, Hamblin WK (SEPM Society for Sedimentary Geology), pp 98–107.
38. Blair TC, McPherson JG (1994) Alluvial fans and their natural distinction from rivers based on morphology, hydraulic processes, sedimentary processes, and facies assemblages. *J Sediment Res* 64(3a):450–489.
39. Trampush SM, Huzurbazar S, McElroy B (2014) Empirical assessment of theory for bankfull characteristics of alluvial channels. *Water Resour Res* 50(12):9211–9220.
40. Gaurav K, et al. (2015) Morphology of the Kosi megafan channels. *Earth Surf Dyn* 3(3):321–331.
41. Métivier F, et al. (2016) Geometry of meandering and braided gravel-bed threads from the Bayanbulak Grassland, Tianshan, P. R. China. *Earth Surf Dynam* 4(1):273–283.
42. Chatanantavet P, Lamb MP, Nittrouer JA (2012) Backwater controls of avulsion location on deltas. *Geophys Res Lett* 39(1). doi:10.1029/2011GL050197.
43. Parker G (1976) On the cause and characteristic scales of meandering and braiding in rivers. *J Fluid Mech* 76(3):457–480.
44. VOROSMARTY CJ, FEKETE BM, TUCKER BA (1998) Global River Discharge, 1807-1991, V[ersion]. 1.1 (RivDIS). doi:10.3334/ornldaac/199.
45. Macdonald FA, Swanson-Hysell NL, Park Y, Lisiecki L, Jagoutz O (2019) Arc-continent collisions in the tropics set Earth's climate state. *Science (80-)*.